

Radiative transfer for inhomogeneous atmospheres: RRTM, a validated correlated- k model for the longwave

Eli J. Mlawer, Steven J. Taubman,¹ Patrick D. Brown, Michael J. Iacono,
and Shepard A. Clough

Atmospheric and Environmental Research, Inc., Cambridge, Massachusetts

Abstract. A rapid and accurate radiative transfer model (RRTM) for climate applications has been developed and the results extensively evaluated. The current version of RRTM calculates fluxes and cooling rates for the longwave spectral region (10–3000 cm^{-1}) for an arbitrary clear atmosphere. The molecular species treated in the model are water vapor, carbon dioxide, ozone, methane, nitrous oxide, and the common halocarbons. The radiative transfer in RRTM is performed using the correlated- k method: the k distributions are attained directly from the LBLRTM line-by-line model, which connects the absorption coefficients used by RRTM to high-resolution radiance validations done with observations. Refined methods have been developed for treating bands containing gases with overlapping absorption, for the determination of values of the Planck function appropriate for use in the correlated- k approach, and for the inclusion of minor absorbing species in a band. The flux and cooling rate results of RRTM are linked to measurement through the use of LBLRTM, which has been substantially validated with observations. Validations of RRTM using LBLRTM have been performed for the midlatitude summer, tropical, midlatitude winter, subarctic winter, and four atmospheres from the Spectral Radiance Experiment campaign. On the basis of these validations the longwave accuracy of RRTM for any atmosphere is as follows: 0.6 W m^{-2} (relative to LBLRTM) for net flux in each band at all altitudes, with a total (10–3000 cm^{-1}) error of less than 1.0 W m^{-2} at any altitude; 0.07 K d^{-1} for total cooling rate error in the troposphere and lower stratosphere, and 0.75 K d^{-1} in the upper stratosphere and above. Other comparisons have been performed on RRTM using LBLRTM to gauge its sensitivity to changes in the abundance of specific species, including the halocarbons and carbon dioxide. The radiative forcing due to doubling the concentration of carbon dioxide is attained with an accuracy of 0.24 W m^{-2} , an error of less than 5%. The speed of execution of RRTM compares favorably with that of other rapid radiation models, indicating that the model is suitable for use in general circulation models.

1. Introduction

A new rapid radiative transfer model (RRTM) has been developed for application to general studies of atmospheric radiative transfer and for implementation in dynamical models ranging from single-column to general circulation models. The objective in the development of RRTM has been to obtain an accuracy in the calculation of fluxes and cooling rates consistent with that of the best line-by-line models. RRTM utilizes the correlated- k method [Ambartzumian, 1936; Arking and Grossman, 1972; Wang *et al.*, 1976; Goody *et al.*, 1989; Lacis and Oinas, 1991; Fu and Liou, 1992], selected for its potential to provide the required accuracy and computational efficiency and, importantly, its direct adaptability to multiple-scattering calculations. RRTM has as its foundation the line-by-line radiative transfer model (LBLRTM) [Clough *et al.*, 1992; Clough and Iacono, 1995], which provides the absorption coefficients for the relevant k distributions. The accuracy of these absorp-

tion coefficients has been established by numerous high-resolution validations of LBLRTM with measurements, particularly those performed in the longwave region as part of the Atmospheric Radiation Measurement (ARM) [Stokes and Schwartz, 1994] Program. These validations provide a traceable link from RRTM to observations done at high spectral resolution.

In the current version of RRTM, absorption due to water vapor, carbon dioxide, ozone, nitrous oxide, methane, CFC-11, CFC-12, CFC-22, and CCl_4 is considered. Accurate calculation of the radiative effect of these gases necessitates dividing the longwave region into a series of spectral bands, each of which contains strong absorption bands due to a limited number of gases. The effect of the key absorbers in each spectral band is treated with high accuracy, with a less detailed procedure employed for computing the absorption due to minor absorbing species in the band.

The flux and cooling rate results from RRTM are validated against the same quantities obtained directly from LBLRTM. This enables the critical evaluation of the results of the model for each of its spectral bands for a wide range of atmospheric conditions. It is essential in evaluating a radiative transfer model to consider not only the resultant fluxes and cooling rates but also their sensitivity to variations in relevant physical

¹Now at Geophysical Fluid Dynamics Laboratory, Princeton, New Jersey.

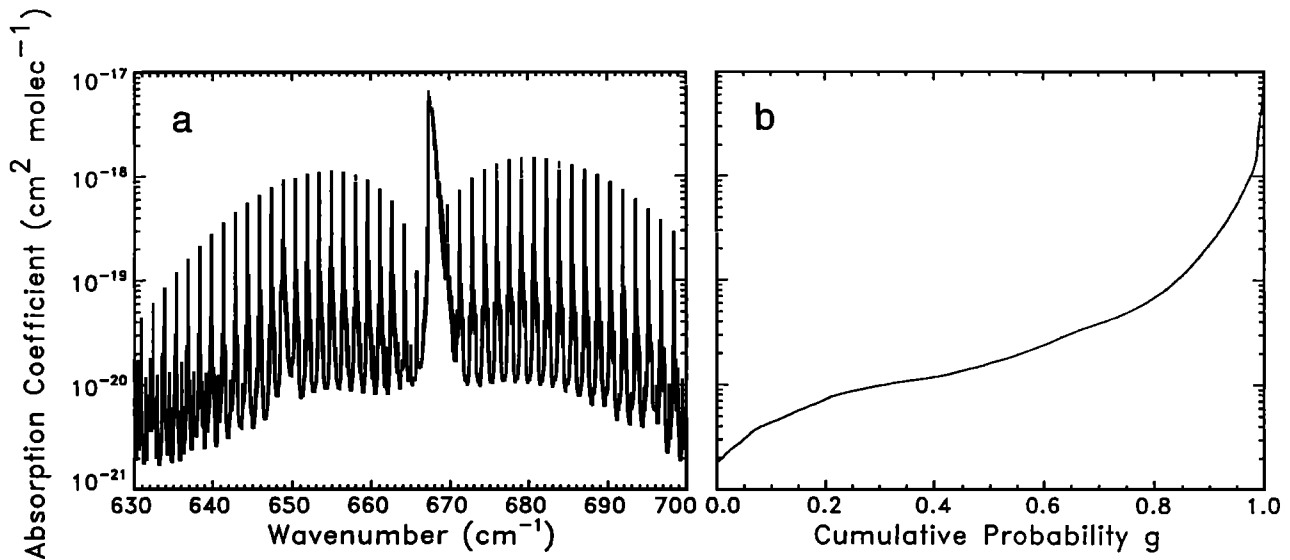


Figure 1. Absorption coefficients due to carbon dioxide for a layer ($P = 507$ mbar) in the midlatitude summer atmosphere for the spectral range $630\text{--}700\text{ cm}^{-1}$ (a) as a function of wavenumber and (b) after being rearranged in ascending order.

quantities. The performance of RRTM over ranges of temperature, water vapor abundance, and ozone abundance has been studied by applying the model to a variety of realistic atmospheric profiles. The performance with respect to the abundances of other species has been analyzed by introducing incremental changes in the profiles of these species. Of particular interest in this regard are the results of the model for the doubling of the CO_2 abundance from current levels.

In section 2 we consider the k -distribution method for a homogeneous layer and its application to the calculation of the radiative transfer for inhomogeneous atmospheres in the context of the correlated- k approach. The development strategy for RRTM is discussed in section 3. Section 3.1 contains a summary of the LBLRTM model and its related validations with observations. In section 3.2 aspects of RRTM related to the calculation of optical depths for an arbitrary atmosphere are described, including the use of LBLRTM for the generation of the needed k distributions. Section 3.3 describes the radiative transfer algorithm in RRTM with emphasis on the method used for the determination of the Planck function. Validations using LBLRTM of flux and cooling rate results for a range of atmospheric profiles are detailed in section 4. Included in this section is a comparison of the results of the two models for the effects of doubling carbon dioxide from present levels. Issues associated with computational efficiency are discussed in section 5. The final section of the paper provides a summary and details the anticipated future direction for the development of RRTM.

2. The k Distributions and the Correlated- k Method

The correlated- k method is an approximate technique for the accelerated calculation of fluxes and cooling rates for inhomogeneous atmospheres. This method is capable of achieving an accuracy comparable with that of line-by-line models with an extreme reduction in the number of radiative transfer operations performed. The radiative transfer operations for a given homogeneous layer and spectral band are carried out

using a small set of absorption coefficients that are representative of the absorption coefficients for all frequencies in the band. The spectral absorption coefficient $k(\nu)$ varies irregularly with wavenumber ν and therefore is not directly suited to the determination of representative values. However, by rearranging the absorption coefficients in ascending order, a characteristic value can be specified for any segment of the now smoothly varying function. Mathematically, this is accomplished by mapping the absorption coefficients $k(\nu)$ from spectral space to a space defined by a variable g (i.e., $k(\nu) \rightarrow k(g)$), where $g(k)$ is the fraction of the absorption coefficients in the set smaller than k . The function $g(k)$ is often referred to as the cumulative probability function. An example of one such mapping is shown in Figure 1, in which absorption coefficients for the spectral range $630\text{--}700\text{ cm}^{-1}$, shown in Figure 1a, undergo a transformation into the space defined by the variable g (Figure 1b). The perspective of the mapping transformation, $\nu \rightarrow g$ [West *et al.*, 1990], from which the k -distribution $k(g)$ is obtained, is a critical element in the development of the current model.

The effect of this reordering is simply a rearrangement of the sequence of terms in the integral over wavenumber in the radiative transfer equations. Therefore radiative transfer in g space can be performed as in monochromatic models. This can be seen by examining the expression for the spectrally averaged outgoing radiance from an atmospheric layer,

$$\bar{R}'_{\nu_1\nu_2} = \frac{1}{\nu_2 - \nu_1} \int_{\nu_1}^{\nu_2} d\nu \left(R_0(\nu) + \int_{T_\nu}^1 [B(\nu, \theta(T_\nu)) - R_0(\nu)] dT' \right). \quad (1)$$

In this expression, ν_1 and ν_2 are the beginning and ending wavenumbers of the spectral interval, R_0 is the radiance incoming to the layer, $B(\nu, \theta)$ is the Planck function at wavenumber ν and temperature θ , T_ν is the transmittance for the

layer optical path, and T'_ν is the transmittance at a point along the optical path in the layer. Under the assumptions that (1) the Planck function varies linearly along the absorbing path in the layer and (2) the layer is homogeneous with respect to pressure, temperature, and species distribution with a characteristic absorption coefficient for the layer, this expression becomes

$$\bar{R}'_{\nu_1, \nu_2} = \frac{1}{\nu_2 - \nu_1} \int_{\nu_1}^{\nu_2} d\nu \left[B_{\text{eff}}(\nu, T_\nu) + [R_0(\nu) - B_{\text{eff}}(\nu, T_\nu)] \exp\left(-k(\nu, P, \theta) \frac{\rho \Delta z}{\cos \phi}\right) \right], \quad (2)$$

where $B_{\text{eff}}(\nu, T_\nu)$ is an effective Planck function for the layer that varies with the layer's transmittance in a manner that ensures continuity of flux across layer boundaries for opaque conditions. (For further explanation of $B_{\text{eff}}(\nu, T_\nu)$, see *Clough et al.* [1992].) In (2) the dependence of the transmittance in equation (1) has been rewritten in terms of the absorption coefficient $k(\nu, P, \theta)$ at layer pressure P and temperature θ , the absorber density ρ in the layer, the vertical thickness Δz of the layer, and the angle ϕ of the optical path. Under the mapping $\nu \rightarrow g$, this becomes

$$\bar{R}'_{\nu_1, \nu_2} = \int_{g_1}^{g_2} dg \left[B_{\text{eff}}(g, T_g) + [R_0(g) - B_{\text{eff}}(g, T_g)] \exp\left(-k(g, P, \theta) \frac{\rho \Delta z}{\cos \phi}\right) \right], \quad (3)$$

where all the terms in (2) with a dependence on ν have been transformed using the mapping $\nu \rightarrow g$. Despite the noncontinuous nature of the effective Planck function with respect to g , the smooth monotonically increasing behavior of the function $k(g)$ results in (3) being amenable to approximation. This is accomplished by partitioning the domain of the variable g into subintervals, each corresponding to a limited range of $k(g)$ values, and determining a characteristic value κ_j of the absorption coefficient for each subinterval. This characteristic value is used to compute the outgoing radiance for the entire subinterval. The resulting radiances, weighted by the sizes W_j of their respective subintervals ($\sum W_j = 1$), are summed to yield an approximation to the average radiance (1):

$$\bar{R}'_{\nu_1, \nu_2} \cong \sum_j W_j R'_j = \sum_j W_j \left[B_{\text{eff},j} + (R_0 - B_{\text{eff},j}) \exp\left(-\kappa_j \frac{\rho \Delta z}{\cos \phi}\right) \right]. \quad (4)$$

The only error introduced in this procedure is due to the use of single κ_j , R_j , and $B_{\text{eff},j}$ values for each subinterval instead of the full set of $k(\nu)$ and R_ν values. There is no error caused by the reordering procedure. Therefore only the desire for an increase in computational efficiency can diminish the accuracy of this method, which is potentially unlimited.

The method is extended to obtain the radiative transfer for vertically inhomogeneous atmospheres by dividing the atmosphere into layers, each treated as described above, and using the outgoing radiance at each value of g as the incoming radiance for the same g value for the adjacent layer. This procedure treats each subinterval in an equivalent manner as a

spectral point is treated in a monochromatic radiative transfer method. Under conditions such that the mapping $\nu \rightarrow g$ is identical for adjacent layers, or equivalently that the k distribution in a given layer is fully correlated in spectral space with the k distribution in the next layer, the extension of this method to inhomogeneous atmospheres is exact; hence this approach is referred to as the correlated- k method. In general, these conditions do not hold. As pressure, temperature, and relative molecular concentrations change from layer to layer, each $k(\nu)$ value will be affected differently. As a result, the spectral elements that contribute to a subinterval of the k distribution for one homogeneous layer will not be mapped to the corresponding subinterval for a different atmospheric layer, and therefore performing radiative transfer through the atmosphere for a single subinterval will not correspond to a fixed set of frequencies. This affects the accuracy of the radiance calculation since, for each layer, the transmittance that acts on the incoming radiance in general will not be perfectly matched with that radiance since the two quantities will be associated with different sets of spectral elements. The magnitude of the resulting error is dependent on the extent to which the mappings $\nu \rightarrow g$ for successive atmospheric layers are correlated. This inaccuracy is generally mitigated by the limited altitude regime over which the atmosphere changes from opaque to transparent and is typically small, especially if the spectral bands are chosen to have homogeneity of contributing species and radiative transfer properties. However, as a consequence of variations of the $\nu \rightarrow g$ mapping for an inhomogeneous atmosphere, the correlated- k method is an approximate treatment of the radiative transfer.

The lack of correlation in the mappings for consecutive layers and the use of single κ_j , R_j , and $B_{\text{eff},j}$ values for each subinterval in the layer are two important sources of error in the correlated- k method. The use of a single fixed mapping in a spectral band for all atmospheric layers would eliminate the correlation error since each subinterval would correspond to the same set of frequencies at all altitudes. The absorption coefficients for the spectral elements in any subinterval would, in general, have a greater range of values in this method than in the correlated- k method, causing an increase in the magnitude of the error due to using a single κ_j for the subinterval. It would be possible to minimize this increase in error by judiciously choosing the layer at which the single $\nu \rightarrow g$ mapping is defined, but whether the increase in this error would outweigh the elimination of the correlation error has not been explored in this work and is a possible subject of future study.

3. Model Development Strategy

Numerous radiative transfer models have been developed for climate applications. Band models [e.g., *Goody*, 1952; *Kiehl and Ramanathan*, 1983; *Crisp et al.*, 1986] are capable of providing accurate results in clear-sky conditions. However, since these models do not possess detailed information about the absorption coefficient distribution, their formalism does not readily lend itself to the calculation of radiative transfer for scattering atmospheres, which is highly dependent on the magnitude of local absorption. Approaches to the accelerated calculation of radiative transfer that have detailed dependence on absorption coefficients, such as the correlated- k method utilized for RRTM and a related method, exponential sum fitting of transmittances [*Lacis and Hansen*, 1974; *Wiscombe and*

Evans, 1977; Edwards and Slingo, 1996], are fully compatible with accelerated multiple-scattering methods.

There are a number of issues associated with the development of rapid radiation models using the correlated- k method and RRTM, in particular, that are important to emphasize. Each correlated- k model must include a procedure to account for variations in a band's absorption coefficient with pressure and temperature. A common method is to scale a reference set of κ_j values (or a function of the κ_j values) by an appropriate function of pressure or temperature. Alternatively, RRTM performs linear interpolation using stored sets of κ_j values, which are obtained from k distributions that have been calculated for the full range of atmospheric conditions of interest. Linear interpolation is utilized extensively in RRTM, effectively eliminating discreteness effects. This also enables the model to accommodate microlayering, which is important in modeling atmospheric inhomogeneities associated with surface/atmosphere and cloud/atmosphere interfaces. The generation of the many k distributions needed, however, is a significant overhead cost involved in the development of RRTM and similar models. It is important that this development effort not serve as a disincentive to the regeneration of the needed parameterizations as more accurate versions of spectral parameter databases become available. For RRTM this is addressed through the implementation of development tools that to a large extent automate the calculation of κ_j values, facilitating their regeneration as required.

A critical element for the model is the method used for performing the radiative transfer for a spectral band with multiple active species. The development of an accurate and computationally efficient approach to this problem has proven to be a challenge for rapid radiation models, including those using the correlated- k approach. Correlated- k models generally have either sacrificed accuracy to preserve computational speed by simply adding the independent contributions of the active species or have maintained model accuracy but with a dramatically increased number of operations to compute the needed optical depths. In RRTM the problem of overlapping bands is dealt with by the introduction of a parameter that allows any combination of two overlapping species to be analyzed accurately and efficiently.

The loss of spectral information when utilizing the mapping $\nu \rightarrow g$ to create a k distribution impedes the use of the nongrey information inherent in other physical quantities, such

as the Planck function. This can result in models treating these quantities as though they had no spectral dependence, i.e., completely grey, with a consequent loss of accuracy. In RRTM, all spectrally dependent physical quantities are utilized in each spectral band in a manner consistent with their respective correlations with the spectral distribution of the band's absorption coefficients. This includes the Planck function, the contribution of minor species to absorption in the band, and the effect of the water vapor self-continuum. (In addition, the contribution of the self-continuum to the optical depth is included in a way that correctly takes into account its quadratic dependence on water vapor abundance.) Details of these procedures appear below.

Last, in order for a model using the correlated- k method to accurately compute cooling rates in the middle and upper atmosphere, high resolution is needed in the part of the k distribution corresponding to values of g near unity. This high resolution in g space is difficult to achieve while maintaining speed of execution. This is handled in RRTM by the division of the k distribution into subintervals of decreasing size with respect to g , with high resolution only at the upper end of the k distribution. This arrangement allows accurate determination of middle atmosphere cooling rates while preserving the speed of the model.

3.1. Relationship Between RRTM and LBLRTM

The fundamental role of LBLRTM in the development of RRTM is indicated schematically in Figure 2. The first of the two major components of this relationship is the use of LBLRTM to obtain the absorption coefficients required to form the k distributions. This establishes direct traceability from the absorption coefficients used in RRTM to high-resolution validations performed on the calculations of LBLRTM with observational data. For the current version of RRTM, the κ_j values are based on the 1992 HITRAN line parameter database [Rothman *et al.*, 1992] and the water vapor continuum model CKD_2.1 [Clough *et al.*, 1989a; 1992]. Figure 2 also indicates the other major component of the foundational relationship, the use of fluxes and cooling rates calculated using LBLRTM to validate the results of RRTM. As indicated in this figure, the calculations of RRTM are greatly accelerated relative to LBLRTM due to the reduction in the number of radiative transfer operations performed.

The line-by-line model LBLRTM is based on the model

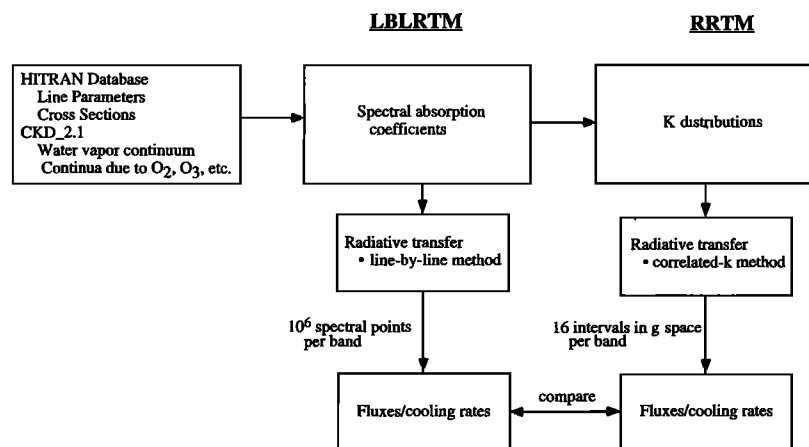


Figure 2. Developmental strategy of RRTM.

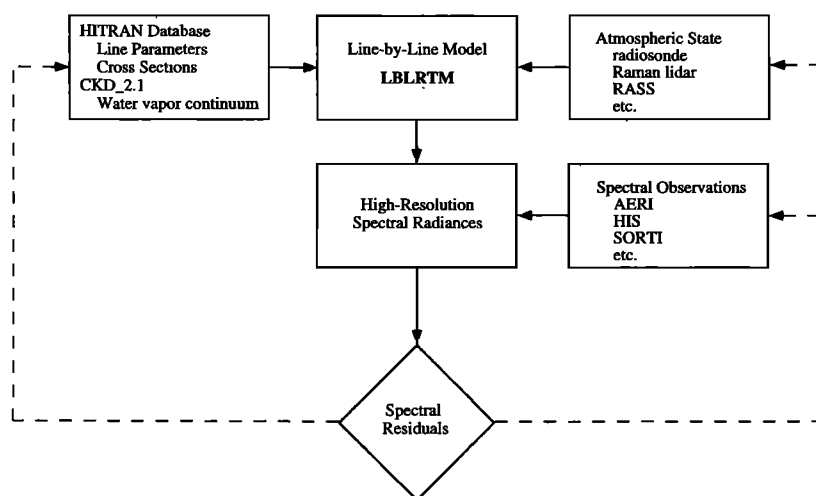


Figure 3. Validation strategy of line-by-line radiative transfer model (LBLRTM).

FASCODE [Clough *et al.*, 1981] and achieves high accuracy with calculational efficiency. The algorithmic accuracy is $\sim 0.5\%$ leading to errors much smaller than those caused by inaccuracies in the line parameters and the line shape, which are the limiting errors in the model. All of the internal parameters of the HITRAN 92 database are utilized, including the coefficient for the self-broadening of water vapor, the pressure shift coefficient, and the half width temperature dependence. LBLRTM includes a complete water vapor continuum model, CKD_2.1, with both self-broadened and foreign-broadened components and incorporates continua due to carbon dioxide, oxygen, and nitrogen. At all pressures, LBLRTM uses the Voigt line shape with a line cutoff of 25 cm^{-1} from the line center. Other model features important in the calculation of optical depths include the treatment of line coupling to second order and the utilization of the TIPS program for the temperature dependence of the line intensities [Gamache *et al.*, 1990]. LBLRTM makes use of an alternative to the “linear in τ ” approximation for vertically inhomogeneous atmospheres, which assumes that the Planck function in a layer varies linearly with optical depth within the layer [Wiscombe, 1976]. A Padé approximation is used to calculate an effective Planck function for each layer by appropriately combining the Planck function at the layer boundary temperature and the Planck function at the mean layer temperature [Clough *et al.*, 1992].

Both upward and downward radiance calculations from LBLRTM have been compared against spectral observations taken by a number of different instruments for a range of atmospheric conditions. The approach taken in the validation of LBLRTM is schematically depicted in Figure 3. The high-resolution spectral residuals obtained from these validations are used to critically analyze the elements involved in the validations: the LBLRTM algorithm and spectral input; the specification of the atmospheric state; and the instrument employed to make the observation. Currently, the limiting element in these validations is the specification of the atmosphere state, particularly with respect to water vapor [Brown *et al.*, 1995].

Extensive validations of downward surface radiances have been done with measurements taken by University of Wisconsin atmospheric emitted radiance interferometer (AERI) [Revercomb *et al.*, 1993]. Figure 4 presents the results of one

such high-resolution comparison, which was performed on a case associated with the SPECTRE (Spectral Radiance Experiment) campaign [Ellingson and Wiscombe, 1996] that was analyzed as part of the Intercomparison of Radiation Codes for Climate Models (ICRCCM) project [Ellingson and Fouquart, 1991]. The measurements shown in Figure 4 were taken in Coffeyville, Kansas, in December 1991 and are associated with an atmosphere with a water vapor column amount of 1.77 cm . The agreement between the observations and the model is within $2\text{ mW sr}^{-1}\text{ m}^{-2}\text{ (cm}^{-1}\text{)}^{-1}$ across most of the measured spectrum. Residuals greater than this do occur in the spectral regions $550\text{--}600\text{ cm}^{-1}$ and $720\text{--}750\text{ cm}^{-1}$ and may be due to an error in the water vapor column amount, which is possibly too low by as much as 10% .

A comprehensive validation effort involving LBLRTM is currently being performed using AERI measurements as part of the ARM program for a Quality Measurement Experiment (QME). The three principal components of the QME are (1) use of LBLRTM to compute spectral radiances, (2) specification of the atmospheric state in the radiating column principally from radiosonde measurements, and (3) use of the ground-based AERI instrument to accurately measure radiances [Brown *et al.*, 1995]. This QME has provided the evidence that the limiting factor in the calculation of atmospheric radiation is the specification of water vapor abundance in the radiating column.

Validations of LBLRTM with upwelling spectral radiances at high altitudes have been performed with measurements from the University of Wisconsin high-resolution interferometer sounder (HIS) [Smith *et al.*, 1983]. The results of one such comparison [Clough *et al.*, 1989b, 1992] indicate good agreement between measurement and calculation, with residuals in brightness temperature less than 2 K across the measured spectrum.

3.2. Generation of k Distributions and Optical Depths for RRTM

There are three important criteria considered in the determination of spectral bands in RRTM: (1) each spectral band can have at most two species with substantial absorption, (2) the range of values of the Planck function in each band cannot be extreme, and (3) the number of bands should be minimal.

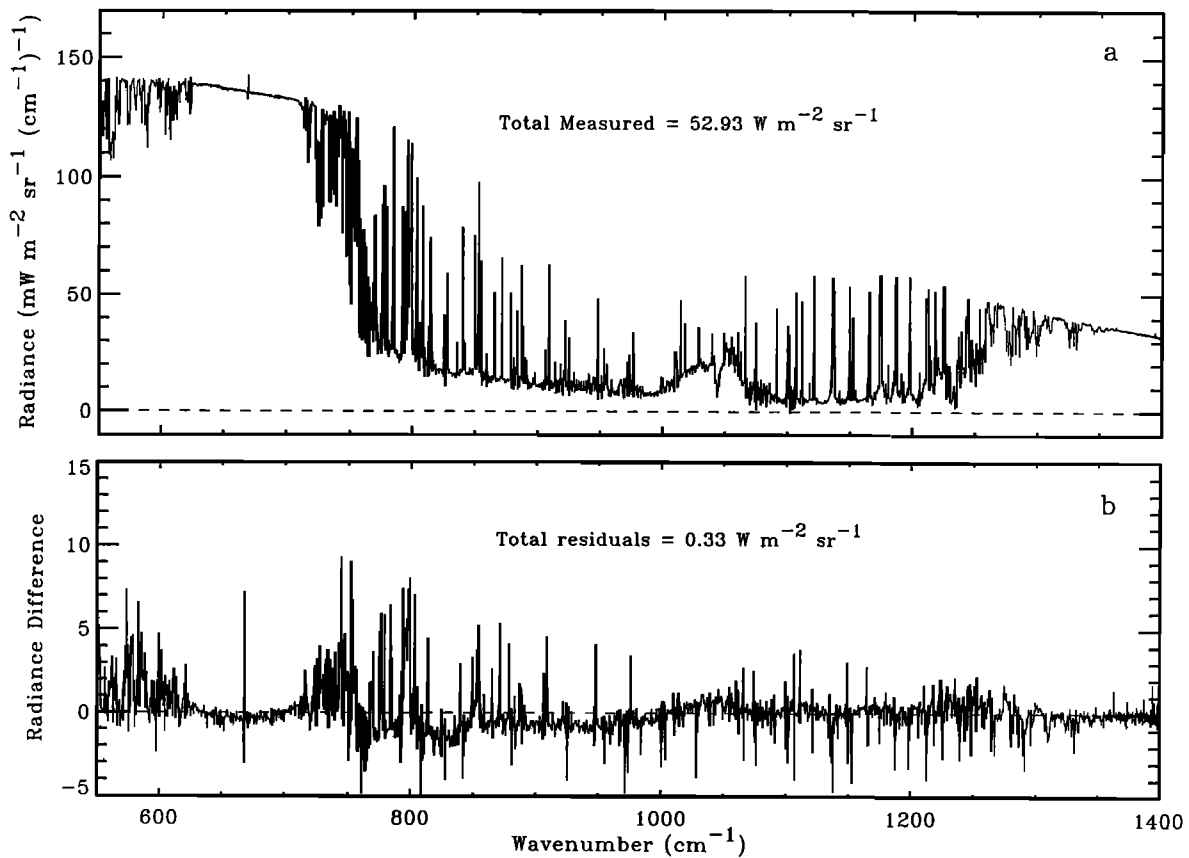


Figure 4. (a) Nadir downward surface radiance spectrum measured with the University of Wisconsin atmospheric emitted radiance interferometer (AERI) and (b) spectral residuals between the measurements and the radiances computed by LBLRTM.

Each species that is responsible for substantial absorption in a spectral band is termed a “key species,” and its effect on radiation is analyzed in detail. Other species in the bands that have small but nonnegligible absorption are referred to as “minor species” and are treated less rigorously. Table 1 presents the spectral bands of RRTM in the longwave region, which are listed with their respective key and minor species. The selection of the spectral regions is facilitated by consideration of the Plates of spectral cooling rate provided by *Clough and Iacono [1995]*, which indicate the spectral domains in which the gases of interest are radiatively important. An important tool in the determination of key and minor species is the product of the integrated line strength of each species with its abundance, which provides an effective indicator of the level of radiative importance of the species within a spectral band.

Because of the large dynamic range in abundance of certain species with altitude, key species in a spectral band are designated for two separate altitude regimes. The transition between the lower and the upper altitude regimes is placed at a level for which the radiative effects for the respective species are relatively small, thereby minimizing potential discreteness. As indicated in Table 1, this transition is located near the tropopause in all bands.

Each spectral band in RRTM is divided into 16 intervals in g space chosen to have modified half Gauss-Legendre quadrature spacing. The boundaries and weights of these intervals are shown in Table 2. The modification to the half Gauss-Legendre spacing, which places seven intervals between $g =$

0.98 and $g = 1.0$, is done to accurately determine the cooling rate for circumstances in which the cooling rate is dominated by the centers of the spectral lines in the band, i.e., the portion of the k distribution having values of g near 1. At any level in an atmosphere, there is only a limited range of absorption coefficient values that provide the main contribution to the cooling rate. The ratio of the highest to the lowest absorption coefficient in this range does not change greatly with altitude, spectral band, or atmospheric profile. Therefore when this range falls near $g = 1$, only a small fraction of the k distribution will contribute due to the rapid increase in the function $k(g)$ at the high end of the k distribution. This creates the necessity for high resolution in g space near $g = 1$. Evidence for this is given by Table 3 [also see *Chou et al., 1994*], which shows some properties of the dominant region of the k distribution in the cooling rate calculation for a number of layers in the midlatitude summer atmosphere for the spectral band 630–700 cm^{-1} . For this table the dominant region is defined as those k values corresponding to a cooling rate greater than 10% of the maximal cooling rate for that level. Table 3 indicates that as altitude increases and the absorption coefficient for which the cooling rate is greatest moves closer to $g = 1$, the fraction of the k distribution contributing significantly to the cooling rate decreases, with less than 1.0% contributing at the highest level ($P = 0.084$ mbar). The variability in the size of RRTM’s subintervals in g space permits suitable accuracy for these cases while preserving computational efficiency for all cases.

Table 1. RRTM Bands

Band Number	Wavenumber Range, cm^{-1}	Species Implemented in RRTM			
		Lower* Atmosphere		Middle/Upper† Atmosphere	
		Key Species	Minor Species	Key Species	Minor Species
1	10–250	H ₂ O		H ₂ O	
2	250–500	H ₂ O		H ₂ O	
3	500–630	H ₂ O, CO ₂		H ₂ O, CO ₂	
4	630–700	H ₂ O, CO ₂		CO ₂ , O ₃	
5	700–820	H ₂ O, CO ₂	CCl ₄	CO ₂ , O ₃	CCl ₄
6	820–980	H ₂ O	CO ₂ , CFC-11,‡ CFC-12	...	CFC-11,‡ CFC-12
7	980–1080	H ₂ O, O ₃	CO ₂	O ₃	
8	1080–1180	H ₂ O	CO ₂ , CFC-12, CFC-22‡	O ₃	
9	1180–1390	H ₂ O, CH ₄		CH ₄	
10	1390–1480	H ₂ O		H ₂ O	
11	1480–1800	H ₂ O		H ₂ O	
12	1800–2080	H ₂ O, CO ₂		...	
13	2080–2250	H ₂ O, N ₂ O		...	
14	2250–2380	CO ₂		CO ₂	
15	2380–2600	N ₂ O, CO ₂		...	
16	2600–3000	H ₂ O, CH ₄		...	

*1050–96 mbar except for band 8 (1050–317 mbar).

†96–0.01 mbar except for band 8 (317–0.01 mbar).

‡Optical depths of these halocarbons are increased to account for other absorption bands of these species that are not implemented.

In the calculation of optical depths for a spectral band in RRTM, a critical element is the determination of the atmospheric parameters upon which the κ_j are dependent. This includes the influence that any such parameter has on the $\nu \rightarrow g$ mapping. The dependence on pressure and temperature is addressed by obtaining and storing values of κ_j on a grid that has spacing fine enough to allow linear interpolation to accurately approximate κ_j for a general atmosphere. The reference κ_j values are stored for 59 pressure levels from 1050–0.01 mbar. Successive pressure levels have a fixed ratio ($\ln^{-1}(0.2) = \sim 1.22$) to ensure equal spacing in log pressure, the variable used for linear interpolation. For each reference pressure level, κ_j values are stored for values of temperature T_{ref} , $T_{\text{ref}} \pm 15$ K, $T_{\text{ref}} \pm 30$ K, where T_{ref} is the temperature corresponding to this pressure in the midlatitude summer profile. Extrapolation is used for the rare cases in which the given pressure or temperature is not within the range of stored values.

Table 2. Boundaries and Weights of Subintervals in g Space Used in RRTM

Subinterval	Initial g Value	Final g Value	Weight
1	0.00000	0.15275	0.15275
2	0.15275	0.30192	0.14917
3	0.30192	0.44402	0.14210
4	0.44402	0.57571	0.13169
5	0.57571	0.69390	0.11819
6	0.69390	0.79583	0.10193
7	0.79583	0.87911	0.08328
8	0.87911	0.94178	0.06267
9	0.94178	0.98427	0.04249
10	0.98427	0.98890	0.00463
11	0.98890	0.99273	0.00383
12	0.99273	0.99576	0.00303
13	0.99576	0.99798	0.00222
14	0.99798	0.99939	0.00141
15	0.99939	0.99993	0.00054
16	0.99993	1.00000	0.00007

For a correlated- k model, it is essential to design a method to accurately and efficiently calculate optical depths in spectral bands that contain more than one significant absorbing species [Goody *et al.*, 1989; Fu and Liou, 1992; Zhu, 1995]. This issue is addressed in RRTM by the inclusion in these bands of an additional variable η , the binary species parameter, in the parameter space associated with the stored κ_j values, i.e., $\kappa_j(\log P, T, \eta)$. This variable, which reflects the relative abundance of the two designated key molecular species, is defined as

$$\eta \equiv \frac{S_1 W_1}{S_1 W_1 + S_2 W_2}, \quad (5)$$

where S_1 and S_2 are the respective integrated line strengths of the two key species in the spectral band, and W_1 and W_2 are their corresponding layer column amounts. A value of η near zero implies that the key species corresponding to index “2” is radiatively dominant, whereas a value near 1 indicates that the first species is dominant. For each reference pressure and temperature, values of κ_j in the relevant bands are stored for atmospheres with values of η spaced appropriately for the utilization of linear interpolation, which is used by the model to compute the κ_j values for the specified atmospheric condition. The use of the parameter η in this way defines a method for overlap bands that yields accurate optical depths and requires twice the number of calculations needed to determine the optical depths for bands with only one contributing species. This ratio of two corresponds to a smaller cost in speed of execution than other methods for accurately handling overlap bands.

In general, η values of 0, 1/8, 2/8, ..., 1 are used in the lower altitude regime and 0, 1/4, 1/2, 3/4, and 1 in the upper regime. In certain bands, $k(g)$ has a strong dependence on η (for a fixed pressure and temperature) near $\eta = 0$ or $\eta = 1$. This extreme nonlinearity leads to inaccuracies when evaluating κ_j values using linear interpolation for layers in an arbitrary atmosphere having these limiting values of η . To address this, in these bands, additional κ_j values are calculated and stored for

Table 3. Dominant Region of k Distribution in the Cooling Rate Calculation for Selected Layers in the MLS Atmosphere for the Spectral Range 630–700 cm^{-1}

Layer Pressure, mbar	Range of Absorption Coefficient for Substantial Cooling, $\text{cm}^2 \times 10^{-20}$	Ratio of Upper to Lower Value in Range	g Values of Upper and Lower Ends of Range	Percentage of k Distribution in Range
20.97	0.0368–1.08	29.4	0.153–0.879	72.6
7.70	0.0873–14.3	163	0.576–0.984	40.8
2.63	0.226–34.7	15.4	0.796–0.989	19.3
0.24	2.2–292	133	0.942–0.998	5.6
0.14	9.14–246	27.0	0.984–0.998	1.4
0.08	56.4–2580	45.7	0.993–0.999	0.6

MLS, midlatitude summer.

layers having values of η in these regions. For example, for band 3 (500–630 cm^{-1}) in the lower atmosphere, reference values of κ_j are obtained at $\eta = 0.9875$ due to the behavior of the absorption coefficient function near $\eta = 1$.

In the development of RRTM, the process of precalculating reference κ_j values for a band begins with the generation of optical depths by LBLRTM (for the specified atmospheric conditions and species abundances) at spectral intervals no greater than 1/4 of the mean spectral line half width over the band. For these calculations the abundances of all species not determined by the value of η are set to their respective abundances in the midlatitude summer atmospheric profile, and the optical depths calculated exclude the contributions of the water vapor self-continuum. An effective absorption coefficient is obtained from each optical depth τ from the relation

$$\bar{\kappa} = \frac{\tau}{W}, \quad (6)$$

where the effective column amount W for the layer is defined for a single key species as

$$W = W_1 \quad (7a)$$

and for binary species as

$$W = W_1 + \left(\frac{S_2}{S_1}\right) W_2. \quad (7b)$$

The resulting absorption coefficients are sorted in ascending order using a sorting routine developed by Chen [Goody *et al.*, 1989]. Finally, κ_j values are obtained by averaging the $k(g)$ values in each of the 16 subintervals, thereby including the contributions from every absorption coefficient in each subinterval. This equal weighting of all $k(g)$ values in the method for the determination of κ_j values differs from similar methods used elsewhere, most notably transmission-weighted averaging [Lacis and Oinas, 1991] and Planck weighting of the transmittance [Chou *et al.*, 1994]. The method used in RRTM avoids an additional interpolation variable, the absorber amount, in the calculation of κ_j values while providing an accurate determination of the average transmission over many scales in absorber amount. In the linear regime the transmittance obtained from a stored κ_j value is equal to the average transmittance of all the spectral elements in the corresponding subinterval.

The κ_j values needed for radiative transfer in RRTM are obtained from the stored κ_j values by linear interpolation in log pressure, temperature, and if appropriate, the binary species parameter η . The absorption coefficients resulting from

these interpolations are multiplied by the appropriate effective column amount for the layer of the arbitrary atmosphere to yield optical depths. In the current version of the model, optical depths obtained by this procedure include the spectral line contributions from the major species and the contributions of the foreign water vapor continuum, which have been grouped together due to their linear dependence on water vapor abundance.

In all bands except band 2 (250–500 cm^{-1}), the above procedure provides results consistent with RRTM's accuracy objectives. In this band, however, the stored absorption coefficients deviate from linearity in log pressure significantly, which leads to an inaccuracy in the determination of values of κ_j when using linear interpolation. Because of the high values of the Planck function in this band, this inaccuracy causes relatively large errors in the radiance calculations. To reduce this error and to conform more closely to the dependence on log pressure exhibited by the stored data, an interpolation in the square root of log pressure is used for this band. This anomalous behavior of the pressure dependence has not yet been explored in detail.

The contribution of the water vapor self-continuum to the optical depth is included by a separate procedure due to its quadratic dependence on water vapor abundance. This proce-

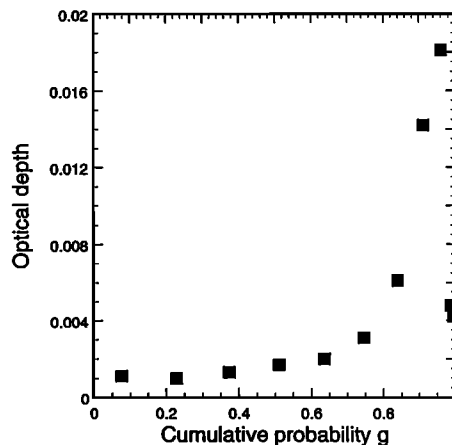
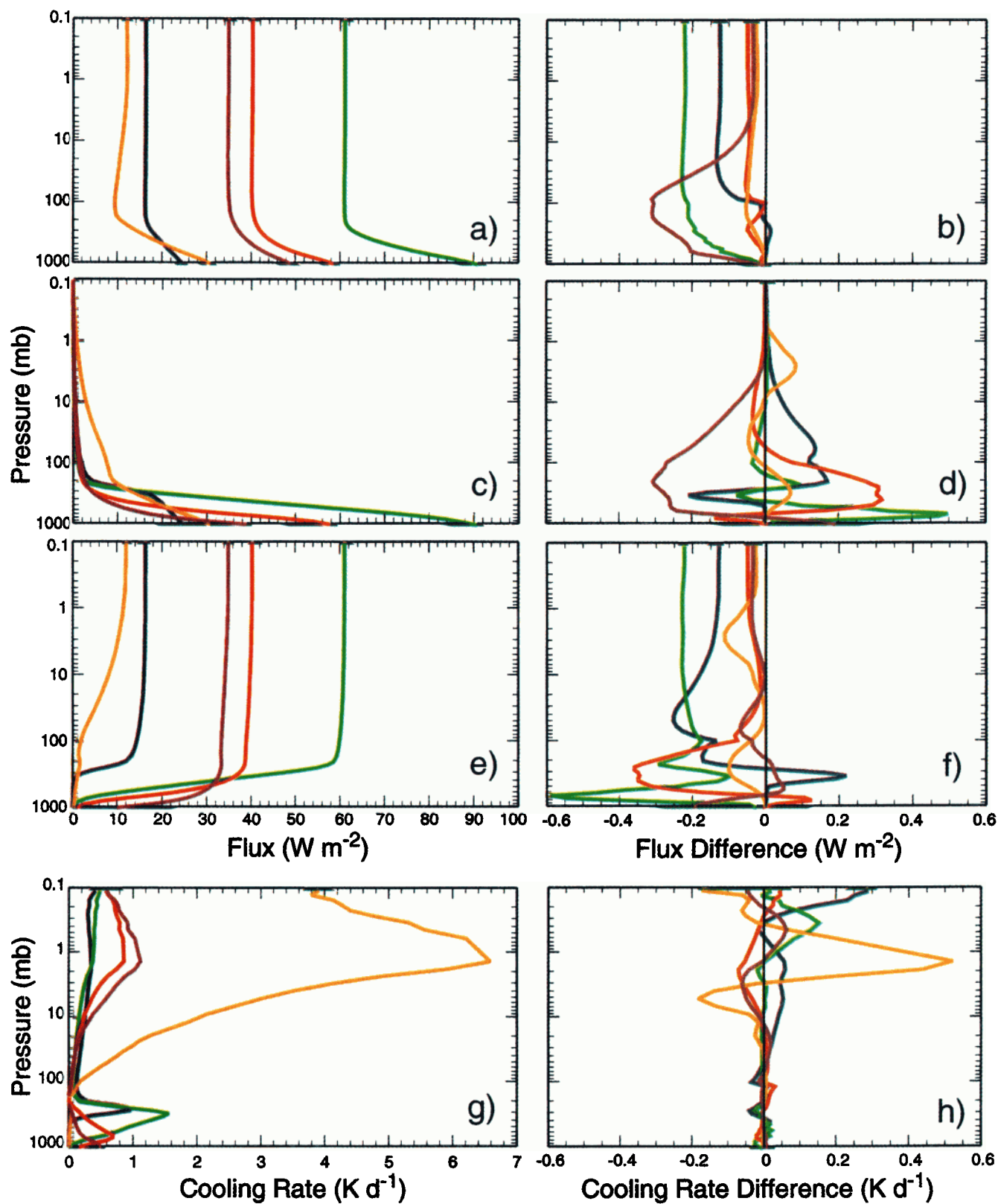


Figure 5. Results of applying the mapping $\nu \rightarrow g$ due to all absorbers in the spectral range 980–1080 cm^{-1} for a layer in the midlatitude summer atmosphere to the optical depths for that layer due to CO_2 . The results are averaged for each subinterval in g space and plotted at the midpoint of the subinterval.



— 10-250 cm^{-1} — 250-500 cm^{-1} — 500-630 cm^{-1} — 630-700 cm^{-1} — 700-820 cm^{-1}

Plate 1. Spectrally integrated (a) up, (c) down, (e) net fluxes, and (g) cooling rates for each of bands 1–5 ($10\text{--}820\text{ cm}^{-1}$) calculated by LBLRTM for the MLS atmosphere. Differences between RRTM and LBLRTM for these quantities are shown in Plates 1b, 1d, 1f, and 1h, respectively. All results are plotted as a logarithmic function of pressure.

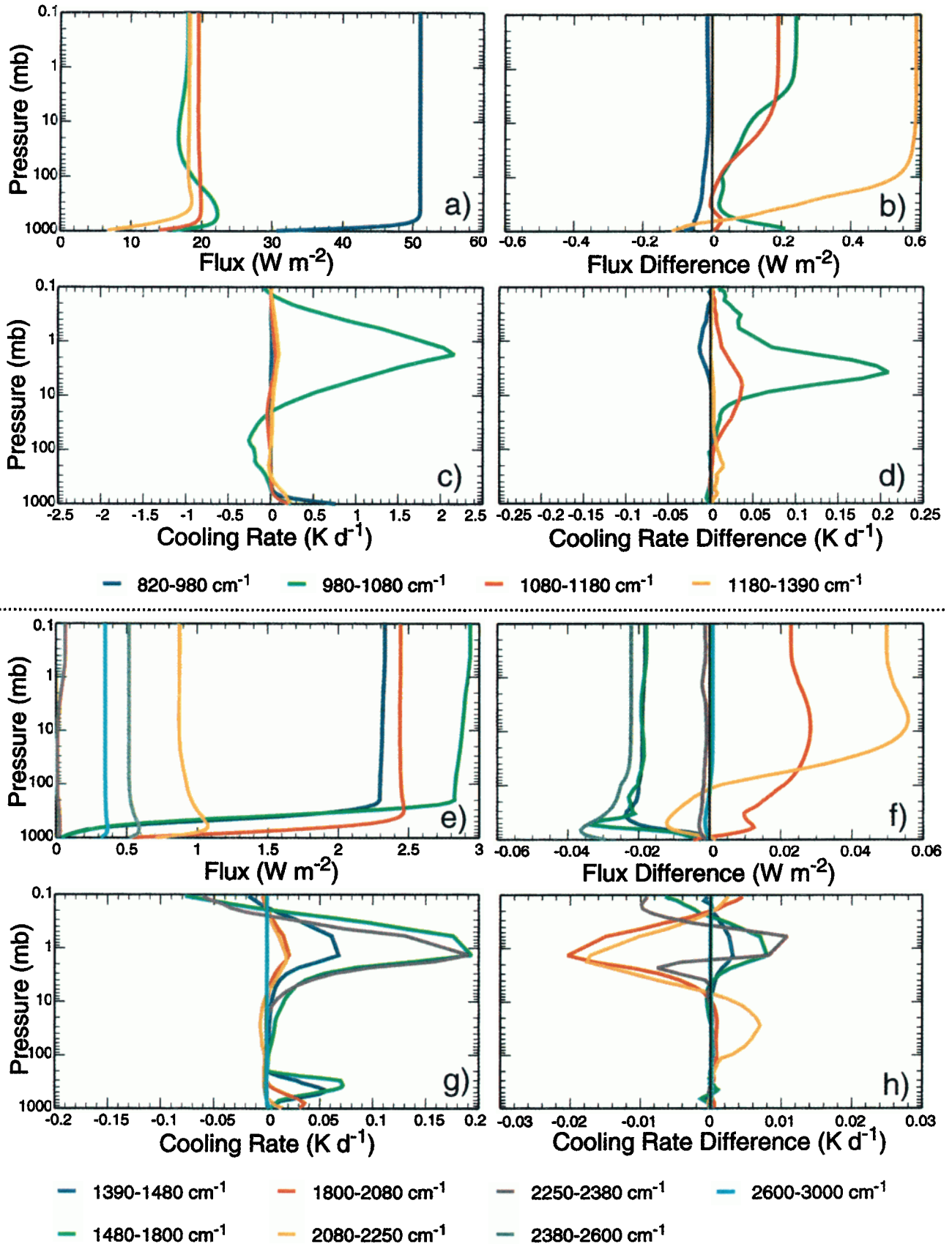


Plate 2. Spectrally integrated (a) net fluxes and (c) cooling rates for each of bands 6–9 (820–1390 cm^{-1}), and (e) spectrally integrated net fluxes and (g) cooling rates for each of bands 10–16 (1390–3000 cm^{-1}) calculated by LBLRTM for the MLS atmosphere. Differences between RRTM and LBLRTM for these quantities are shown in Plates 2b, 2d, 2f, and 2h, respectively. All results are plotted as a logarithmic function of pressure.

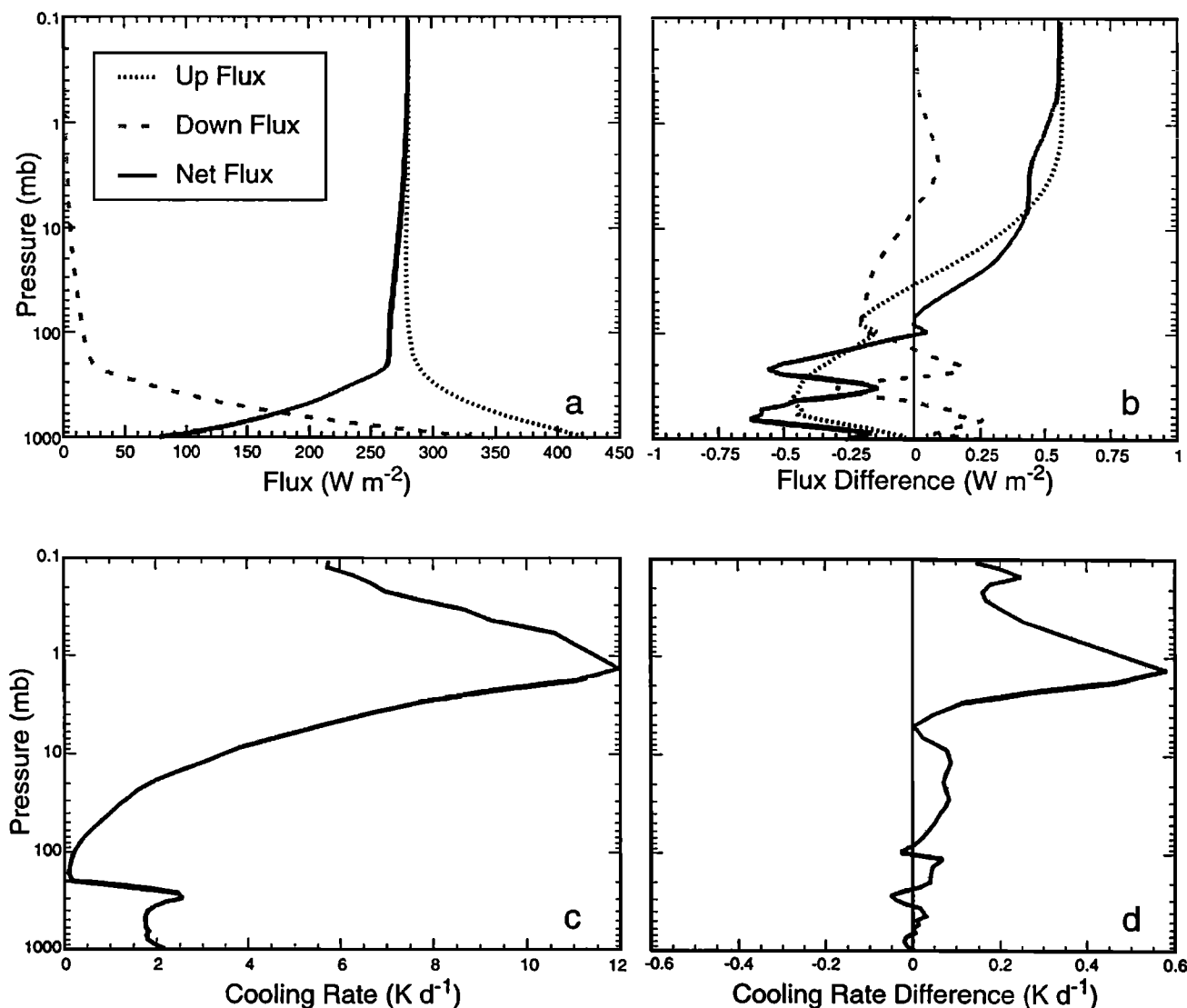


Figure 6. (a) Spectrally integrated longwave up, down, and net fluxes calculated by LBLRTM for the midlatitude summer (MLS) atmosphere, (b) differences in these fluxes between RRTM and LBLRTM calculations, (c) spectrally integrated cooling rates calculated by LBLRTM for the MLS atmosphere, and (d) differences in these cooling rates between RRTM and LBLRTM as a logarithmic function of pressure.

procedure ensures that the contribution of the self-continuum to the optical depth is included in a manner consistent with the correlation between the absorption spectrum of the self-continuum and the full absorption spectrum in the band. This correlation is accounted for by the determination of the mapping $\nu \rightarrow g$ for all absorbers in each band and the subsequent application of this mapping to the self-continuum absorption coefficients in the band, which allows the computation of an average value $\kappa_{j,\text{self}}$ for each subinterval. Note that the property $\kappa_j < \kappa_{j+1}$, which holds for the absorption coefficients due to the spectral lines and foreign continuum, does not hold for the values $\kappa_{j,\text{self}}$. Since $\kappa_{j,\text{self}}$ depends on both the mapping $\nu \rightarrow g$ in the band and the values of $k_{\text{self}}(\nu)$, which are temperature dependent, this procedure is done for two reference atmospheric layers from the midlatitude summer atmospheric profile, chosen to have temperatures of 296 and 260 K, respectively. For the given atmospheric conditions, a logarithmic interpolation in temperature is performed between the two reference values to obtain the $\kappa_{j,\text{self}}$ to be used. Finally, the

contribution of the self-continuum to the optical depth is computed by multiplying $\kappa_{j,\text{self}}$ by a scaling factor that depends quadratically on water vapor abundance.

The radiative effects of minor species are also included in a manner that takes into account the correlation between absorption spectrum of each minor species and the full absorption spectrum in the corresponding spectral band. In the current version of RRTM the minor species implemented (and their respective spectral bands) are CFC-11 (820–980 cm^{-1}), CFC-12 (820–980 cm^{-1} , 1080–1180 cm^{-1}), CFC-22 (1080–1180 cm^{-1}), CCl_4 (700–820 cm^{-1}), and the “laser bands” of carbon dioxide (820–980 cm^{-1} , 980–1080 cm^{-1} , 1080–1180 cm^{-1}). For the bands in which carbon dioxide is used as a minor species, the stored values of κ_j for these bands include the contribution of carbon dioxide due to its current abundance (355 ppm at most altitudes) in a midlatitude summer profile, so it is the radiative impact of any change from this concentration that is calculated by the minor species algorithm.

The method for the inclusion of each of the halocarbons

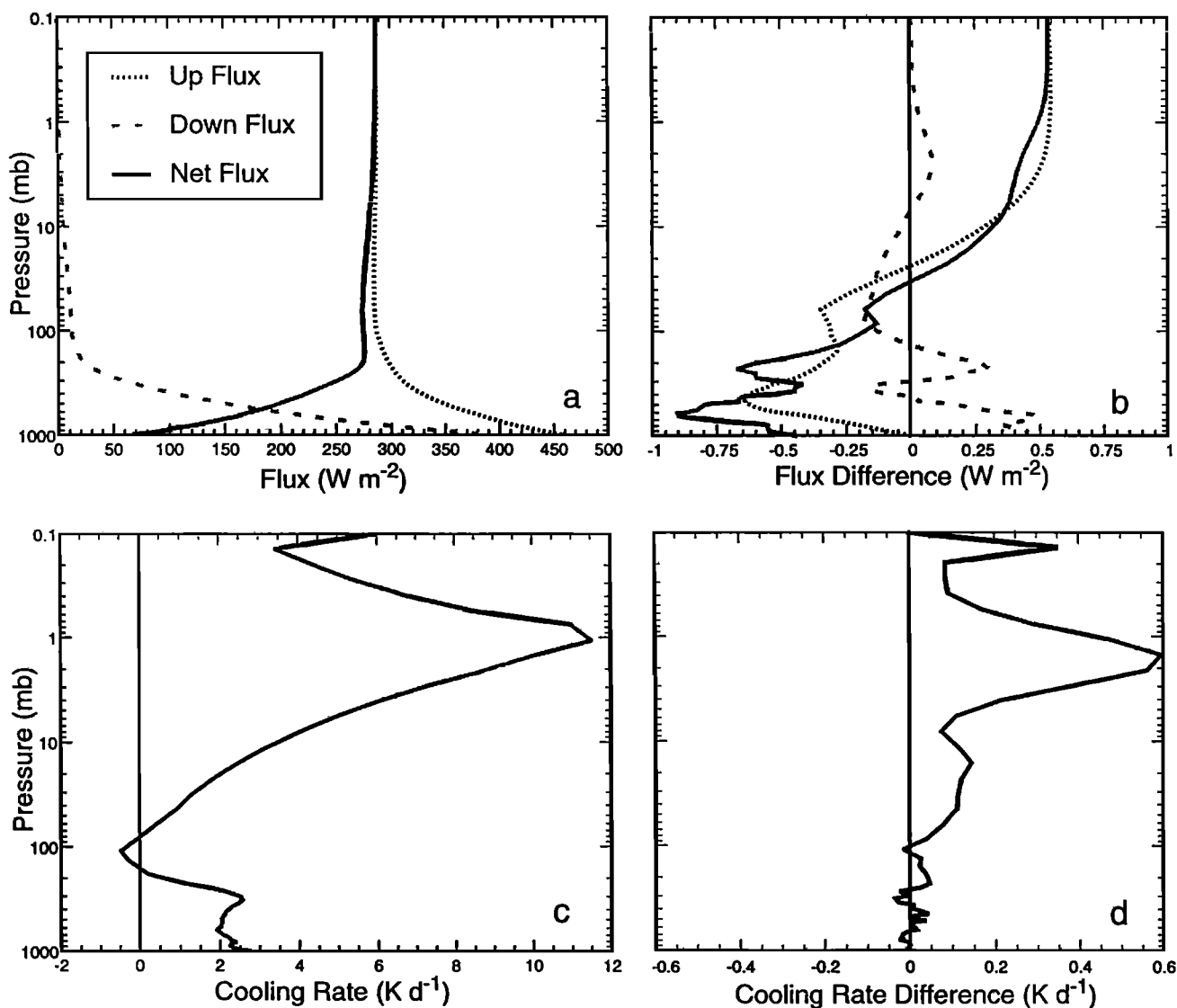


Figure 7. (a) Spectrally integrated longwave up, down, and net fluxes calculated by LBLRTM for the tropical (TR) atmosphere, (b) differences in these fluxes between RRTM and LBLRTM calculations, (c) spectrally integrated cooling rates calculated by LBLRTM for the TR atmosphere, and (d) differences in these cooling rates between RRTM and LBLRTM as a logarithmic function of pressure.

mentioned above is similar to the method used for the contribution of the water vapor self-continuum: the mapping $\nu \rightarrow g$ for all the absorbers in the band for a layer in the midlatitude summer atmosphere is applied to the absorption spectrum of the halocarbon in question, and the results are averaged for each subinterval. This procedure yields values $\kappa_{j,\text{halo}}$. Sufficient accuracy can be obtained with the use of a single mapping for all atmospheric layers (in contrast to the procedure used for the self-continuum). For CFC-11 and CFC-22, these averaged values are increased to account for absorption in spectral bands not explicitly computed in RRTM. (Additional absorption occurs due to CFC-11 for 980–1080 cm^{-1} and 1080–1180 cm^{-1} and due to CFC-22 for 700–820 cm^{-1} , 820–980 cm^{-1} , and 1180–1390 cm^{-1}). The effect of this scaling is to obtain the correct radiative effect of these species for the entire longwave spectrum, although the results are no longer correct for the individual spectral bands.

The contribution of carbon dioxide in the bands in which it is considered a minor species is included by a variation of the

procedure used for the halocarbons. As in that procedure, the mapping $\nu \rightarrow g$ for all the absorbers in a band is applied to the absorption coefficients due to carbon dioxide, and the results are averaged in each subinterval in g space, obtaining values κ_{j,CO_2} . Figure 5 presents the results of this procedure for the 980–1080 cm^{-1} spectral range for a layer in the midlatitude summer atmosphere. Since the contribution in these bands of carbon dioxide (for 355 ppm) is already included in the values of κ_j used, the values κ_{j,CO_2} are multiplied by the layer column amount of carbon dioxide in excess of the column amount corresponding to 355 ppm. Because of the strong dependence of the band strength on temperature the values of κ_{j,CO_2} used for an atmospheric layer are scaled from the stored reference values by a temperature-dependent factor which describes the population of the lower-energy state of the transition that causes the absorption band

$$S'(\theta) = S'(\theta_0) [\exp(-E''/k\theta) / \exp(-E''/k\theta_0)] [\theta_0/\theta], \quad (8)$$

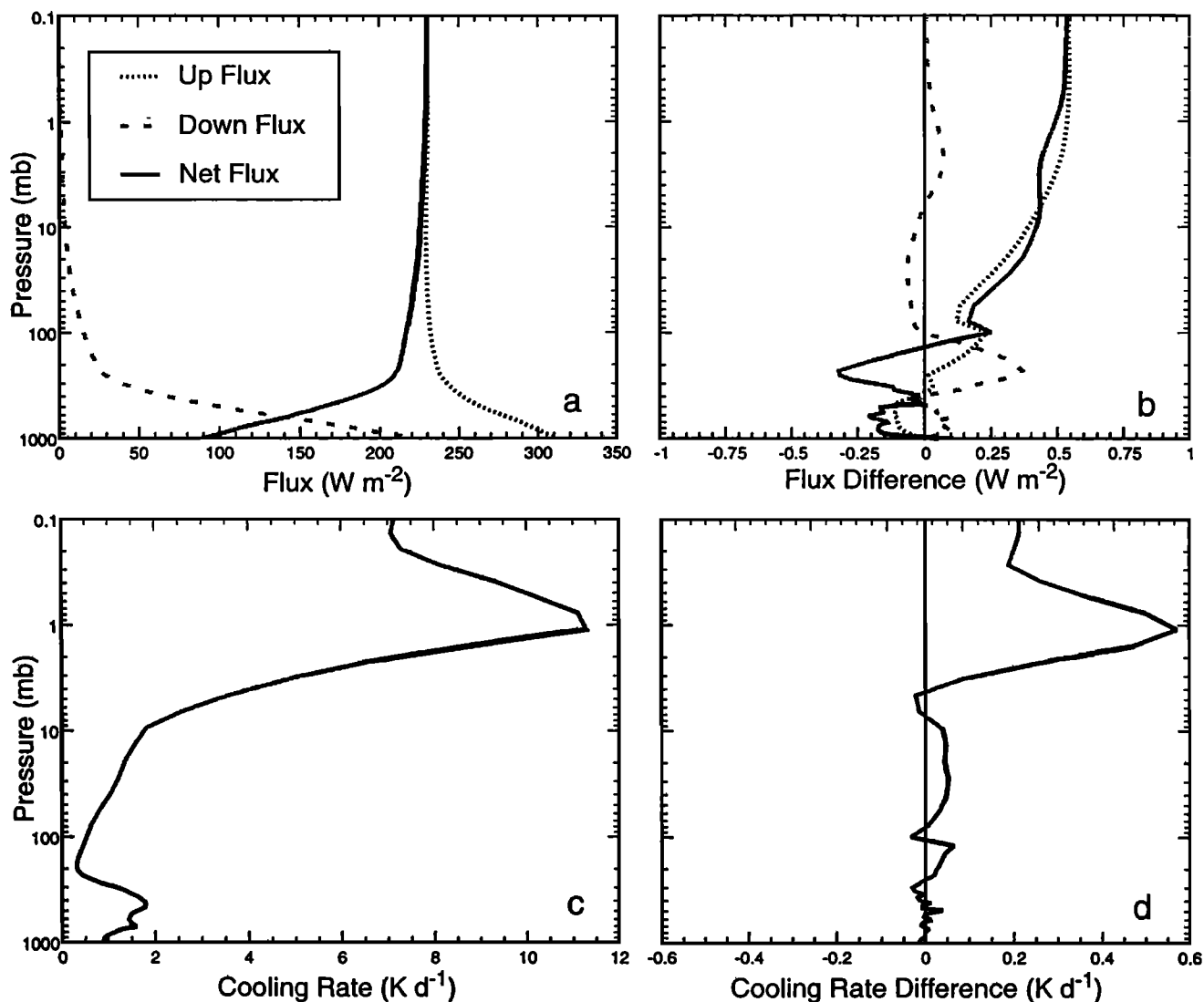


Figure 8. (a) Spectrally integrated longwave up, down, and net fluxes calculated by LBLRTM for the midlatitude winter (MLW) atmosphere, (b) differences in these fluxes between RRTM and LBLRTM calculations, (c) spectrally integrated cooling rates calculated by LBLRTM for the MLW atmosphere, and (d) differences in these cooling rates between RRTM and LBLRTM as a logarithmic function of pressure.

where θ_0 is a reference temperature and E' is the energy of the lower state (1334 cm^{-1}).

3.3. Radiative Transfer Algorithm

For each subinterval in each band, a layer-by-layer radiative transfer calculation is performed. This treats each subinterval, which corresponds to a large number of frequencies in the band, in the same manner as a single spectral point is treated in a line-by-line model. Therefore much of the radiative transfer methodology proven to be accurate in LBLRTM can be used in RRTM. In particular, the same variation of the “linear in τ ” approximation for vertically inhomogeneous atmospheres [Clough *et al.*, 1992] is employed:

$$B_{\text{eff}}(\tau) = \frac{B_{\text{lay}} + 0.2\tau B_{\text{bnd}}}{1 + 0.2\tau}, \quad (9)$$

where B_{lay} and B_{bnd} are, respectively, the Planck functions at the mean layer temperature and the temperature at the layer’s exiting boundary, and τ is the optical depth. The radiative

transfer equation used for each layer and interval can then be written as (see equation (4))

$$R' = R_0 + (B_{\text{eff}} - R_0)A, \quad (10)$$

where R' and R_0 are the outgoing and incoming radiances, respectively, for the subinterval and A is the absorptance. The application of this formalism in RRTM has certain difficulties since the appropriate (layer and level) Planck functions for any subinterval in a band depend on the values of the Planck function evaluated at all frequencies that are associated with that subinterval. Moreover, the mapping $\nu \rightarrow g$ can vary dramatically with atmospheric properties, especially the relative abundance of the band’s key species, thereby limiting the accuracy of approximating the Planck function for the interval by the value of the Planck function at a single “dominant” frequency. This issue is addressed by a two-part procedure. First, the integrated Planck radiance for a band, which is a function only of temperature, is calculated and stored at every 1 K (with linear interpolation used to obtain the corresponding

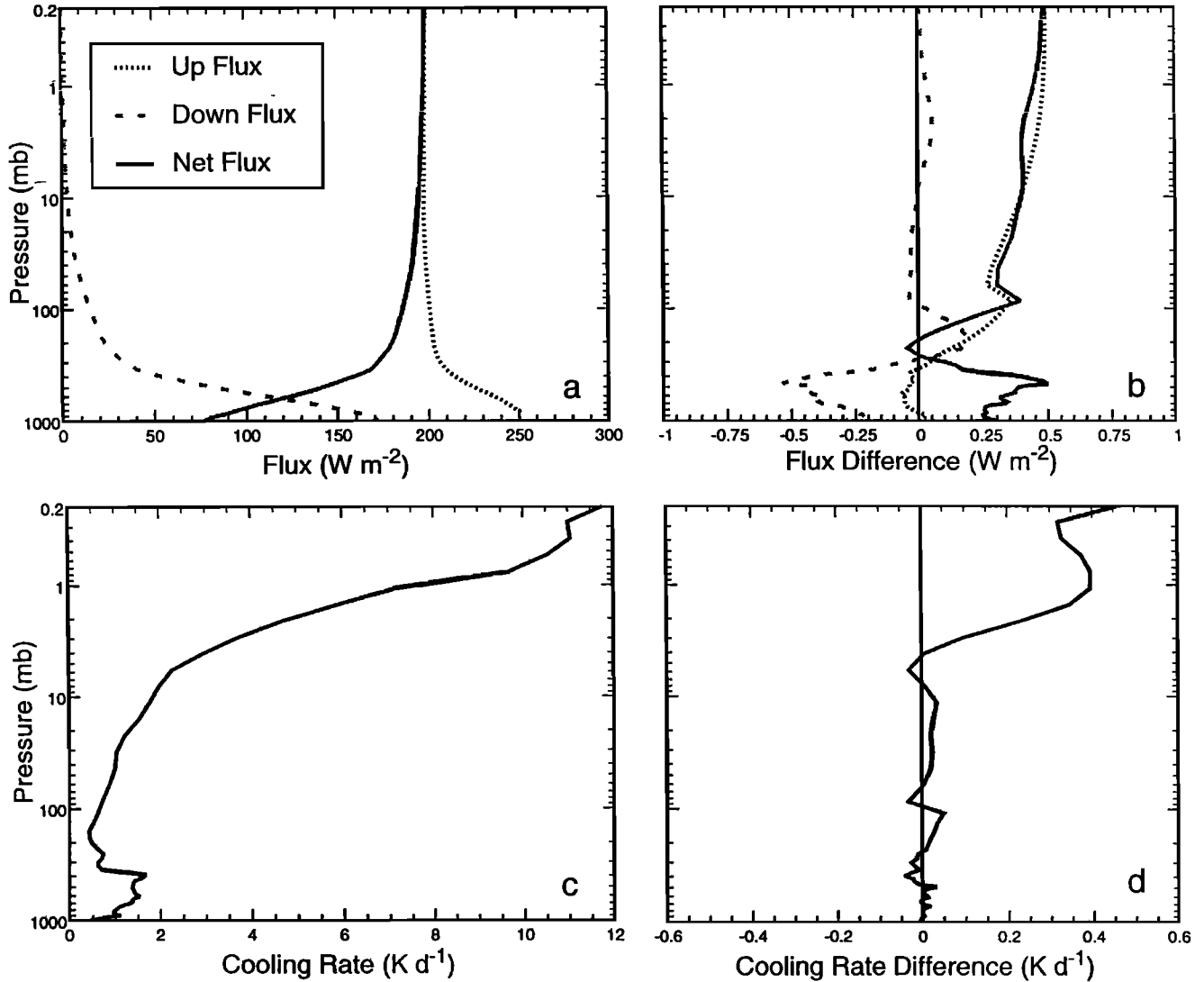


Figure 9. (a) Spectrally integrated longwave up, down, and net fluxes calculated by LBLRTM for the subarctic winter (SAW) atmosphere, (b) differences in these fluxes between RRTM and LBLRTM calculations, (c) spectrally integrated cooling rates calculated by LBLRTM for the SAW atmosphere, and (d) differences in these cooling rates between RRTM and LBLRTM as a logarithmic function of pressure.

value at the given temperature). Second, the fraction of this radiance that is due to the frequencies associated with an interval is defined by the relation

$$f_g \equiv \frac{B_g W_g}{\frac{1}{\nu_2 - \nu_1} \int_{\nu_1}^{\nu_2} B_\nu(T) d\nu}, \quad (11)$$

where B_g is the average Planck function of the frequencies in the interval, W_g is the weight for the interval, and ν_1 and ν_2 are the frequency limits of the band. This fraction depends principally on the mapping $\nu \rightarrow g$, which in turn is most dependent on the ratio of the abundances of the band's key species. For overlap bands, f_g is treated as a function of η and is computed by linear interpolation from stored f_g values calculated for reference values of η . For bands with one key species, f_g is considered constant. All calculations performed to generate reference f_g values for a band are done at a pressure level appropriate for the band and use midlatitude summer atmo-

spheric properties for all unspecified quantities. The Planck function for a subinterval is obtained by multiplying f_g by the integrated Planck radiance for the band. The use of this procedure ensures that the total Planck radiance is correct at every level in each band.

An exception to the procedure described above for the determination of f_g occurs in band 2 ($250\text{--}500\text{ cm}^{-1}$). In this band, the shape of the Planck function changes greatly with altitude. This causes a large difference between values of f_g for layers at different levels in the same atmosphere, behavior otherwise seen only if a band has more than one key absorbing species. For this band therefore, f_g is not considered constant in the lower atmosphere. Instead, values of f_g are computed and stored for a variety of water vapor mixing ratios and an interpolation in this mixing ratio is performed to compute f_g values for an arbitrary atmosphere.

The radiances calculated by the methods described above are integrated (which is approximated by a first-moment Gaussian quadrature) over a hemisphere to yield fluxes. A

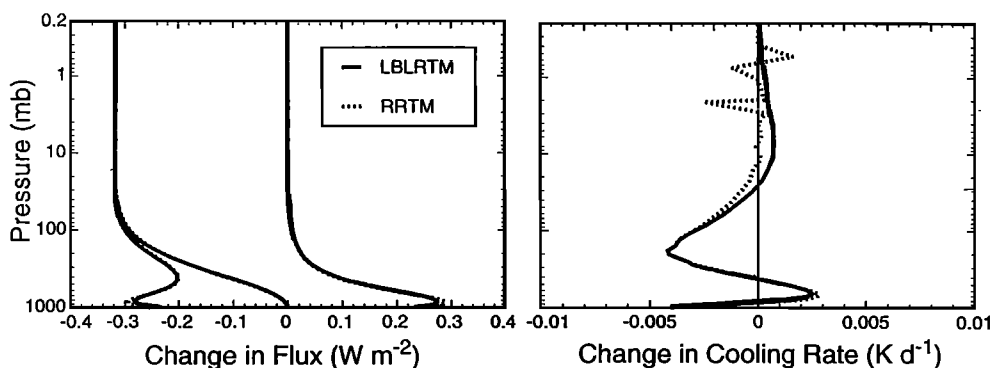


Figure 10. (Left) Contributions to the integrated up, down, and net fluxes and (right) cooling rates due to the halocarbons for the MLS atmosphere in the 820–980 cm^{-1} spectral range as a logarithmic function of pressure.

choice of angular integration options is available. The default option best combines speed and accuracy [Lacis and Oinas, 1991], requiring the performance of only one exponential per interval, layer, and band for the calculation of transmittances at three angles. For this to be possible, the secants of the three angles must satisfy the relationships $\sec(\theta_1) = M_1 \sec(\theta_0)$ and $\sec(\theta_2) = M_2 \sec(\theta_0)$, where M_1 and M_2 are positive integers, implying that the respective transmittances satisfy $T_1 = (T_0)^{M_1}$ and $T_2 = (T_0)^{M_2}$. Values of $\sec(\theta_0)$, M_1 , and M_2 were determined by minimizing the difference between the angular integral and the quadrature approximation to this integral for analytic functions resembling $R(\theta)$, the radiance as a function of angle [Clough *et al.*, 1992]. The values chosen were $\sec(\theta_0) = 1/0.82$, $M_1 = 2$, and $M_2 = 3$, corresponding to zenith angles of 34.9°, 65.8°, and 74.1°, respectively. The second choice available in the model places the angles at which radiances are calculated such that their cosines are equal to the standard ordinate values in first-moment Gaussian quadrature. In this case, the user selects the number of angles n to be analyzed, where $n = 1, 2, 3$, or 4. This second option requires the calculation of n times the number of exponentials needed for the first option, leading to a degradation in speed. For $n = 4$, this method does provide slightly more accuracy than the first choice of angles. The third choice for the angular integration is a variation of the one-angle option described above. Instead of using the standard ordinate position in first-moment quadrature for the cosine of the angle to be evaluated, the cosine of the angle is set to 1/1.66. This approach to the angular integration, referred to as the diffusivity approximation, achieves an accuracy approximately equivalent to that of the two angle quadrature. This option is a useful alternative to the default option, providing roughly a factor of 2 improvement in speed with a decrease in accuracy of about 0.5 W m^{-2} for the longwave region.

4. Validations

The results of an accurate line-by-line (LBL) model for a range of atmospheric profiles provide the best basis to fully judge the accuracy of the algorithm used by a rapid model. Validation using an LBL model is complementary to the use of experimental data, which can be limited in spectral coverage, altitude regime, and range of atmospheric conditions such as water vapor abundance. In addition, the validation of the rapid radiation model by an LBL model does not suffer from prob-

lems due to inaccuracy in the specification of atmospheric state, an issue that critically affects comparisons with observations. Validations using an LBL model can always be done for each spectral band of the rapid model, ensuring that any concordance between the two models is due to the algorithm rather than fortuitous cancellation of errors. An additional critical advantage available only with an LBL validation is the ability to perform incremental validations, in which a comparison is made between two atmospheres that differ solely in a single atmospheric property, such as carbon dioxide abundance.

The validations presented in this section are for both idealized atmospheric profiles and profiles obtained by measurement. The standard profiles analyzed are for the midlatitude summer (MLS), tropical (TR), midlatitude winter (MLW), and subarctic winter (SAW) atmospheres. Also analyzed are the results for profiles from four SPECTRE cases from the ICRCM project. Together, these atmospheres span a wide range of conditions, allowing the accuracy of RRTM to be gauged for different temperature, water vapor, and ozone profiles. Also described in this section are comparisons of the sensitivities of RRTM and LBLRTM to changes in the abundance of certain halocarbons and to a doubling of the carbon dioxide concentration. (All the validations presented below were done using the default angular integration option.)

4.1. Midlatitude Summer Atmosphere

Figure 6 shows the results of the validation of RRTM for the midlatitude summer atmosphere for the full longwave region 10–3000 cm^{-1} . Figure 6b presents the differences between the calculations of RRTM and LBLRTM for up, down, and net flux (defined as up flux minus down flux) as a logarithmic function of pressure. For reference the results of the calculation of these respective quantities by LBLRTM are provided in Figure 6a. The residuals for each of these quantities do not exceed 0.65 W m^{-2} at any altitude and represent only a small percentage of their respective values. Figure 6d indicates that the error in the cooling rate calculation is different in magnitude in the lower and upper altitude regimes. In the lower region the maximum error is less than 0.06 K d^{-1} . The small magnitude of the error is maintained for a large portion of the stratosphere but increases to greater than 0.5 K d^{-1} near 1 mbar. This large error is primarily caused by the calculation in RRTM of downward fluxes in the upper atmosphere due to carbon dioxide in band 4 and ozone in band 7 that are too large

Table 4. Nadir Downward Radiances at the Surface From AERI Measurements, Differences in Downward Radiances Between the Measurement and LBLRTM, and Differences in Downward Radiances Between RRTM and LBLRTM for Four Atmospheres From SPECTRE Campaign

Band Number	Spectral Range, cm^{-1}	Integrated Radiance, $\text{W m}^{-2} \text{sr}^{-1}$											
		Case 1 $-1.77 \text{ cm H}_2\text{O}$			Case 2 $-0.55 \text{ cm H}_2\text{O}$			Case 3 $-0.73 \text{ cm H}_2\text{O}$			Case 4 $-0.95 \text{ cm H}_2\text{O}$		
		AERI	LBLRTM	RRTM-LBLRTM	AERI	LBLRTM	RRTM-LBLRTM	AERI	LBLRTM	RRTM-LBLRTM	AERI	LBLRTM	RRTM-LBLRTM
4	630–700	9.499	-0.015	0.004	8.672	-0.035	0.004	7.556	0.009	0.003	7.926	0.006	0.003
5	700–820	9.061	0.067	0.07	6.655	0.081	-0.029	5.642	0.135	-0.028	6.898	0.259	0.00
6	820–980	2.658	-0.097	-0.007	0.798	-0.039	-0.063	0.718	0.05	-0.035	1.224	0.103	-0.04
7	980–1080	1.582	-0.017	-0.036	1.033	-0.02	-0.037	0.881	0.056	-0.041	1.039	0.034	-0.037
8	1080–1180	1.115	-0.004	-0.011	0.488	-0.012	-0.048	0.408	0.025	-0.031	0.622	0.036	-0.031
9	1180–1390	6.253	-0.033	0.014	4.33	-0.094	-0.06	3.304	-0.019	0.039	4.349	0.052	0.029
10	1390–1480	2.721	0.077	-0.001	2.218	0.021	0.002	1.629	0.013	0.003	1.836	0.012	-0.003
11	1480–1800	5.439	0.184	-0.002	4.32	0.049	-0.001	3.116	0.054	0.002	3.42	0.008	-0.004
12	1800–2080	1.444	-0.012	0.00	0.95	-0.02	-0.004	0.641	0.00	-0.008	0.882	0.01	-0.009
13	2080–2250	0.196	-0.002	-0.003	0.122	-0.003	-0.002	0.08	-0.001	0.00	0.124	0.002	-0.001
14	2250–2380	0.21	0.003	0.001	0.155	0.002	0.00	0.10	0.005	0.00	0.115	0.002	0.00
15	2380–2600	0.037	0.003	0.002	0.027	0.001	0.001	0.018	0.001	0.00	0.026	0.002	0.00
4–15	630–2600	40.215	0.154	0.031	29.768	-0.069	-0.236	24.094	0.328	-0.096	28.462	0.525	-0.092

AERI, atmospheric emitted radiance interferometer; LBLRTM, line-by-line radiative transfer model; SPECTRE, Spectral Radiance Experiment.

(see Plates 1h and 2d). Even though the differences between the calculations in RRTM and LBLRTM are small, they cause an appreciable error in the cooling rate due to the low atmospheric density present in the upper atmosphere. An approach to the reduction of this error in the computation of downward flux is currently being investigated.

Plates 1 and 2 present the comparison between the flux and cooling rate calculations of RRTM and LBLRTM for the 16 spectral bands in RRTM. These plates show that RRTM achieves accuracy on a band-by-band basis, indicating that the agreement between the models in Figure 6 is not due to cancellation of large errors of opposite signs from the individual bands, although some cancellation does occur.

Plate 1 shows the results for the first 5 bands, spanning the spectral range 10–820 cm^{-1} . For these bands, the errors in the quantities directly calculated, the upward and downward flux, are presented in Plates 1b and 1d, respectively, with their respective reference LBLRTM calculations given in Plates 1a and 1c. No error in these bands exceeds 0.5 W m^{-2} . The comparison for the net flux is shown in Plates 1e and 1f. The greatest error is for band 2 (250–500 cm^{-1}), in which the difference between the net flux computed by RRTM and LBLRTM has a maximum of 0.6 W m^{-2} near 700 mbar, principally due to an error in the calculation of downward flux. The corresponding percentage error in net flux for this band is consistent with other spectral bands, suggesting that even

though the radiative transfer algorithm in this band has the unique features previously described, this error is most likely due to the general approximations involved in the correlated- k method. Plate 1h indicates that the error in the cooling rate calculation for each band is less than 0.05 K d^{-1} below 10 mbar. The cooling rate error in the upper atmosphere is dominated by the error in band 4 (630–700 cm^{-1}), which alone can be greater than 0.5 K d^{-1} . This error, along with similar errors in other bands, is due to the calculation of downward fluxes at these altitudes that are too large.

Plate 2b shows the errors in net flux for the spectral bands in RRTM that lie in the longwave atmospheric window region, with the corresponding reference LBLRTM calculations given in Plate 2a. The largest of the errors shown is for band 9 (1180–1390 cm^{-1}) which has a value near 0.6 W m^{-2} in the stratosphere. This error is caused by the lack of spectral correlation of the k distributions for layers in the troposphere. Near the surface, water vapor is the key absorber in this band and dominates the mapping $\nu \rightarrow g$, with a value of 0.998 for the binary species parameter η in the boundary layer. (For this band in this altitude regime, water vapor is species 1 and methane is species 2 in the definition of η in (5).) Because of the decrease in the water vapor concentration higher in the atmosphere the importance of methane in determining the mapping $\nu \rightarrow g$ increases, as demonstrated by a value of 0.133 for η at 150 mbar. This causes a lack of correlation in the k

Table 5. Effects on Fluxes Due to the Halocarbons at Top of Atmosphere (TOA), Tropopause, and Surface for MLS Atmosphere

	Fluxes, W m^{-2}						
	TOA	Tropopause			Surface		
	Up	Up	Down	Net	Up	Down	Net
LBLRTM, MLS (10–3000 cm^{-1})	283.3	286.0	20.6	265.4	423.6	345.6	78.1
LBLRTM, MLS (760–1340 cm^{-1})	128.0	132.3	2.0	130.3	151.1	77.2	73.9
LBLRTM, (MLS + HCs) – MLS	-0.32	-0.26	0.016	-0.28	0.0	0.23	-0.23
RRTM, (MLS + HCs) – MLS	-0.32	-0.24	0.019	-0.26	0.0	0.25	-0.25

Table 6. Effects on Fluxes and Cooling Rates Due to Doubled Concentrations of CO₂ From Current Levels (355 ppm) at TOA, Tropopause, and Surface for MLS Atmosphere

Band Number	Wavenumber Range, cm ⁻¹	Fluxes, W m ⁻²												Cooling Rates, K d ⁻¹										
		TOA Net			Up			Down			Net			Surface Net			Tropopause			Surface				
		LBLRTM	RRTM	Diff	LBLRTM	RRTM	Diff	LBLRTM	RRTM	Diff	LBLRTM	RRTM	Diff	LBLRTM	RRTM	Diff	LBLRTM	RRTM	Diff	LBLRTM	RRTM	Diff		
3	500–630	-1.20	-1.34	-0.14	-1.19	-1.27	0.70	0.80	-0.10	-1.89	-2.07	0.18	0.04	0.01	0.01	0.01	0.01	0.00	0.01	0.01	0.00	0.01	-0.017	-0.016
4	630–700	0.57	0.58	0.01	-0.33	-0.31	0.38	0.41	-0.03	-0.71	-0.72	0.01	0.04	0.03	0.01	0.01	0.00	0.00	-0.019	-0.019	0.00	-0.002	-0.002	-0.003
5	700–820	-1.74	-1.87	-0.13	-1.86	-1.89	0.61	0.62	-0.01	-2.47	-2.52	0.05	0.90	0.92	0.02	0.02	0.00	0.00	0.007	0.007	0.00	-0.054	-0.053	-0.005
6	820–980	-0.19	-0.23	-0.04	-0.17	-0.21	0.01	0.00	-0.18	-0.22	0.04	0.33	0.33	0.00	0.00	0.00	0.00	0.00	-0.001	-0.001	0.00	-0.001	-0.001	-0.005
7	980–1080	-0.12	-0.09	0.03	-0.16	-0.15	0.00	0.00	-0.16	-0.16	0.00	0.32	0.30	0.02	0.02	0.00	0.00	0.00	0.001	0.001	0.00	0.001	0.001	0.000
8	1080–1180	-0.04	-0.04	0.00	-0.04	-0.04	0.00	0.00	-0.05	-0.04	0.01	0.09	0.07	0.02	0.02	0.00	0.00	0.00	0.000	0.000	0.00	0.001	0.001	0.000
9	1180–1390	-0.02	0.00	0.02	-0.02	-0.02	0.00	0.00	-0.02	0.00	0.00	0.00	0.00	0.00	0.00	0.00	0.00	0.00	0.000	0.000	0.00	0.000	0.000	0.000
12	1800–2080	-0.05	-0.03	0.02	-0.04	-0.03	0.00	0.00	-0.04	-0.03	0.01	0.02	0.00	0.00	0.00	0.00	0.00	0.00	0.000	0.000	0.00	0.000	0.000	0.000
13	2080–2250	-0.04	0.00	0.04	-0.04	-0.04	0.00	0.00	-0.04	0.00	0.00	0.04	0.00	0.00	0.00	0.00	0.00	0.00	0.000	0.000	0.00	0.000	0.000	0.000
14	2250–2380	0.01	0.01	0.00	0.00	0.00	0.00	0.00	-0.01	0.00	0.00	0.00	0.00	0.00	0.00	0.00	0.00	0.00	0.000	0.000	0.00	0.000	0.000	0.000
15	2380–2600	-0.02	-0.07	-0.05	-0.01	-0.07	0.00	0.00	-0.01	-0.07	0.01	0.01	0.07	0.07	0.00	0.00	0.00	0.00	0.000	0.000	0.00	0.000	0.000	0.001
Total	10–3000	-2.84	-3.08	-0.24	-3.88	-3.95	1.70	1.84	-5.58	-5.82	1.81	1.69	1.69	1.69	0.00	0.00	0.00	-0.001	-0.001	0.002	-0.075	-0.075	-0.076	-0.076

distributions for successive layers throughout the lower atmosphere, leading cumulatively to a moderate error at the tropopause. Plates 2c and 2d present the cooling rate results for these bands. As before, all the cooling rate errors in the lower atmosphere are small. In the stratosphere the error in the cooling rate approaches 0.2 K d⁻¹ for the spectral band 980–1080 cm⁻¹.

Plates 2f and 2h present the error in net flux and cooling rate, respectively, for the final seven spectral bands in RRTM. In these bands the magnitudes of these errors are small due to the low values of the calculated fluxes and cooling rates (Plates 2e and 2g).

4.2. Tropical, Midlatitude Winter, and Subarctic Winter Atmospheres

Validations of RRTM performed using the TR, MLW, and SAW atmospheric profiles demonstrate that the model provides accurate results for atmospheres with a wide range of water vapor column amounts and temperature profiles. The flux and cooling rate comparisons for these atmospheres are similar to those of the MLS atmosphere. Figure 7, which shows the errors in flux and cooling rate for the TR atmosphere, is nearly identical to Figure 6. Errors in up, down, and net flux (Figure 7b), which do not exceed 1.0 W m⁻² at any altitude, are slightly greater than those for the MLS atmosphere. However, the associated percentage errors for these two atmospheres are comparable. Figure 7d, which shows the error in cooling rate, strongly resembled Figure 6d, with small (less than 0.05 K d⁻¹) errors in the troposphere and a maximum error of 0.6 K d⁻¹ in the upper atmosphere. The band-by-band errors for net flux and cooling rate for the TR atmosphere are similar to those for the MLS atmosphere (Plates 1 and 2) and are not reproduced here.

Figures 8 and 9 present the flux and cooling rate results for the MLW and SAW atmospheres, respectively. In the upper atmosphere these results are similar to those for the MLS and TR atmospheres, with an error of 0.5 W m⁻² at the top of the atmosphere. In the troposphere, however, the error in net flux becomes increasingly more positive as the amount of water vapor and temperature decrease (i.e., for the sequence TR → MLS → MLW → SAW). This is in part a result of the net flux in band 2 (250–500 cm⁻¹) having smaller negative errors for the cases with less water vapor due to smaller errors in the determination of the optical depths. The cooling rate results for the MLW and SAW atmospheres, as shown in Figures 8d and 9d, respectively, exhibit similar behavior as the results for the MLS and TR atmospheres.

4.3. SPECTRE Atmospheres

RRTM has also been validated using atmospheric profiles obtained by field experiments. Table 4 presents the results of downward surface radiance calculations for four profiles from the SPECTRE campaign. The profiles were obtained during autumn in the midwestern United States and range in water vapor column amount from 0.55 cm to 1.77 cm, with three of the four profiles containing temperature inversions. Also listed in Table 4 for these profiles are the results of integrating the spectral downwelling surface radiance measurements from the AERI interferometer to the spectral bands of RRTM. (Note that since 520 cm⁻¹ was the lowest wavenumber for which a measurement was obtained, only the results for the bands beginning after this wavenumber are presented in Table 4.) The results in Table 4 indicate that the differences between the

RRTM and LBLRTM calculations are, in general, smaller in magnitude than the differences between the AERI measurements and the LBLRTM calculations. In all but one case, the total error ($630\text{--}2600\text{ cm}^{-1}$) is less for RRTM, and the average magnitudes of the differences for the four cases is $0.115\text{ W m}^{-2}\text{ sr}^{-1}$ for RRTM and $0.296\text{ W m}^{-2}\text{ sr}^{-1}$ for the AERI measurements. It is again important to emphasize that performing validations with spectral observations requires the measurement of the atmospheric state. Extensive validations of this type indicate that the limiting error in these validations is due to the specification of the water vapor profile.

Obtaining this level of accuracy for the SPECTRE cases is dependent on the inclusion in RRTM of the radiative effects of the halocarbons. For cases having little water vapor, absorption due to these species has increased importance in the window region of the spectrum. For instance, for the spectral interval $820\text{--}980\text{ cm}^{-1}$ the average difference between the calculations of RRTM and LBLRTM of the four cases is $0.036\text{ W m}^{-2}\text{ sr}^{-1}$. The average difference increases to $0.089\text{ W m}^{-2}\text{ sr}^{-1}$ if the effects of CFC-11 and CFC-12 are removed.

4.4. Addition of Halocarbons

The method described in section 3.2 for the inclusion of minor species makes it possible to analyze the incremental effect of the addition of halocarbons to the atmosphere. Figure 10 and Table 5 present a validation of this type of sensitivity analysis, in which the halocarbons CFC-11, CFC-12, CFC-22, and CCl_4 were added to the midlatitude summer atmosphere in the amounts specified by a two-dimensional chemistry model [Ko *et al.*, 1993] (see Clough and Iacono [1995, Figure 2]). For this incremental addition the effect on the fluxes and cooling rates computed by RRTM for the longwave region is similar to that of LBLRTM. For CFC-11 and CFC-22 the results for the individual spectral bands (not presented) will have greater errors than the total results since the absorption of these species in their respective bands is scaled to account for absorption in other spectral regions. It should be noted that the version of LBLRTM used to obtain the results presented in Figure 10 and Table 5 employ the CKD_2.0 water vapor continuum model.

4.5. Doubled CO_2

To assess the sensitivity of RRTM to changes in CO_2 concentrations, both RRTM and LBLRTM were used to calculate the differences in fluxes and cooling rates resulting from doubling concentrations of CO_2 from its current level of 355 to 710 ppm. The results of this comparison for the top of the atmosphere, tropopause, and surface are presented in Table 6. It is important to note that these results provide a test of two separate methods utilized in RRTM to account for the radiative effect of gases. In the spectral bands in which CO_2 is considered a key species (bands 3, 4, 5, 12, 14, and 15), doubling the CO_2 abundance fundamentally alters the mapping $\nu \rightarrow g$. As indicated by Table 6, the aggregate results for these bands are accurate, with an error of less than 10%. Satisfactory results are also attained for the individual bands containing substantial energy. (Less important bands, such as band 15, for unknown reasons do not have very accurate results.) There is an additional radiative effect of the increased abundance in the window region of the spectrum (bands 6, 7, and 8) [Kratz *et al.*, 1991], which includes the “laser bands” of CO_2 . In these three spectral bands, CO_2 is considered a minor species, and its radiative effect is analyzed by the second method used in

RRTM, as described in section 3.2. As can be seen in Table 6, this method provides results with an accuracy comparable to that obtained with the first, more rigorous, method.

The totals given in Table 6 for the longwave region of the spectrum indicate that RRTM provides roughly equivalent results to those of LBLRTM for the doubling of CO_2 concentrations, with errors of less than 10%. It should be noted that the version of LBLRTM used to obtain the results presented in Table 6 employed the CKD_2.0 water vapor continuum model.

5. Model Structure and Computational Efficiency

RRTM has been developed to have a modular structure. Each of its components can easily be extracted from the model and used in other computations. The module that computes the optical depths for a given atmospheric profile has been incorporated into a ARM collaborative radiative transfer model, 3ARM [Bergstrom *et al.*, 1996]. In addition, a version of RRTM has been developed for incorporation into the CCM2 general circulation model. To facilitate comparisons with LBLRTM (and application of RRTM at ARM Cloud and Radiation Test (CART) bed sites), RRTM has the identical atmospheric input module as LBLRTM. Also important for diagnostic purposes is the option to provide the calculated fluxes and cooling rates for the full longwave region $10\text{--}3000\text{ cm}^{-1}$, the full longwave region plus each individual spectral band, or any individual spectral band. When the output is listed for the full longwave region, a correction is included to include the small terrestrial contribution to the flux and cooling rate from wavenumbers greater than 3000 cm^{-1} .

One of the more computationally expensive operations in radiative transfer models is the exponential, required to obtain a transmittance from an optical depth. To reduce the number of exponential operations that are needed to perform the radiative transfer for an atmosphere, RRTM has special paths that avoid exponentiation for the cases of low and high optical depths. The gain in speed from this approach is significant. For example, in calculating the radiative transfer for the midlatitude summer atmosphere, less than one third of the optical depths are exponentiated to obtain transmittances, allowing only 7% of the total execution time of the radiative transfer module to be used for the performance of exponentials. In addition, this module spends 27% of its execution time computing the needed optical depths, with the remaining 66% devoted to the actual radiative transfer.

Results of timing tests for RRTM indicate that computing the fluxes and cooling rates for a 51-layer atmosphere, which includes the performance of 256 (16 bands \times 16 subintervals) upward and downward radiative transfer calculations per layer, takes 0.06 s on a SPARCserver 1000 (using the default choice of angles). This compares favorably with the other rapid radiative transfer models tested, including the model used in CCM2. Preliminary results of timing comparisons performed between the RRTM and the CCM2 radiation module indicate that RRTM is 30–40% faster on a SPARCserver 1000 and ~50% faster on a CRAY Y-MP for a clear-sky case. Further improvement in the speed of RRTM is possible with the use of the diffusivity angle option instead of the default angle option. This choice reduces the number of radiative transfer operations by a factor of 3 (the number of required optical depths and exponentials remains the same), although there would be a slight decrease in accuracy.

A measure of the computational efficiency of the model that is less machine-dependent than the time of execution is its timing relative to a benchmark routine consisting solely of exponentials, where the number of exponentials performed in this benchmark is equal to the number of transmittances needed to compute the radiative transfer for the given atmosphere. This comparison, where each power that was exponentiated in the benchmark was a unique number with a value near -2 , indicates that the ratio of the times of execution of RRTM and the benchmark routine is 2.5. This benchmark is archived and available to those interested from the authors. RRTM is available from the AER homepage at <http://www.aer.com>.

6. Summary

The evaluation of the flux and cooling rate results of RRTM indicates that the model has an accuracy consistent with line-by-line models. The speed of the model makes it suitable for use in general circulation models, and it is versatile enough to maintain these levels of accuracy and speed for a diverse range of molecular abundances, temperature profiles, and layering schemes.

The development of a rapid radiation model involves a determination of the appropriate balance between speed and accuracy. Given the attainment of the objective of obtaining a model accuracy consistent with line-by-line calculations, there are a number of areas that can be explored to improve the speed of the model. These include reducing the number of subintervals into which some or all of the bands are divided and combining noncontiguous spectral regions having similar absorbers into single spectral bands. Any potential change should be thoroughly investigated to determine its effect on the accuracy of the model.

This model (and its future versions) has the potential to be an effective tool in the study of climate. Toward this end, the authors of this study are currently investigating the effects of improved radiative modeling on feedbacks in the climate system by incorporating RRTM into the general circulation model CCM2. (RRTM is easily adapted to treat clouds in the longwave.) Two issues that are of particular interest in this investigation are (1) the effect of inclusion of the foreign water vapor continuum on surface temperature and on upper tropospheric water vapor fields and (2) the consequences of implementing improvements in the modeling of ozone in the radiative calculation. This investigation will also critically evaluate the accuracy and speed of RRTM relative to the radiation code currently incorporated in this and other global models.

The next phase in the development of RRTM will involve the extension of the algorithm to the shortwave region of the spectrum. The objective of this effort will be, again, to obtain results comparable in accuracy to those of a line-by-line model. When this extension has undergone critical validation, a multiple-scattering capability will be added to RRTM to allow the calculation of fluxes and cooling rates for both clear and cloudy skies.

Acknowledgments. The authors would like to thank Luke Chen for providing the code used to create the k distributions. The authors also wish to acknowledge the contributions of Robert Bergstrom, Ronald Farren, and Richard Goody. This research was supported by the Environmental Science Division of the U.S. Department of Energy under grant DE-FG02-90ER61064 as part of the Atmospheric Radiation Measurement Program.

References

- Ambartunian, V., The effect of the absorption lines on the radiative equilibrium of the outer layers of the stars, *Publ. Obs. Astron. Univ. Leningr.*, 6, 7–18, 1936.
- Arking, A. A., and K. Grossman, The influence of line shape and band structure on temperatures in planetary atmospheres, *J. Atmos. Sci.*, 29, 937–949, 1972.
- Bergstrom, R., S. Kinne, B. Toon, E. J. Mlawer, S. A. Clough, and T. Ackerman, 3ARM—A fast, accurate radiative transfer model for use in climate codes, paper presented at the 6th Atmospheric Radiation Measurement Science Team Meeting, Atmos. Radiat. Meas. Program, San Antonio, Tex., 1996.
- Brown, P. D., S. A. Clough, N. E. Miller, T. R. Shippert, D. D. Turner, R. O. Knuteson, and H. E. Revercomb, Assessment of modeling capability for longwave spectral radiances, paper presented at the IUGG XXI General Assembly, Int. Union of Geod. and Geophys., Boulder, Colo., 1995.
- Clough, S. A., and M. J. Iacono, Line-by-line calculation of atmospheric fluxes and cooling rates, 2, Application to carbon dioxide, ozone, methane, nitrous oxide, and the halocarbons, *J. Geophys. Res.*, 100, 16,519–16,535, 1995.
- Chou, M.-D., W. L. Ridgway, and M. M.-H. Yan, Parameterizations for water vapor IR radiative transfer in both the middle and lower atmospheres, *J. Atmos. Sci.*, 52, 1159–1167, 1994.
- Clough, S. A., F. X. Kneizys, L. S. Rothman, and W. O. Gallery, Atmospheric spectral transmittance and radiance: FASCOD1B, *Proc. Soc. Photo. Opt. Instrum. Eng.*, 277, 152–166, 1981.
- Clough, S. A., F. X. Kneizys, and R. W. Davies, Line shape and the water vapor continuum, *Atmos. Res.*, 23, 229–241, 1989a.
- Clough, S. A., R. D. Worsham, W. L. Smith, H. E. Revercomb, R. O. Knuteson, G. P. Anderson, M. L. Hoke, and F. X. Kneizys, in *IRS '88: Current Problems in Atmospheric Radiation*, edited by J. Lenoble and J. F. Geleyn, pp. 376–379, A. Deepak, Hampton, Va., 1989b.
- Clough, S. A., M. J. Iacono, and J.-L. Moncet, Line-by-line calculations of atmospheric fluxes and cooling rates: Application to water vapor, *J. Geophys. Res.*, 97, 15,761–15,785, 1992.
- Crisp, D., S. B. Fels, and M. D. Schwarzkopf, Approximate methods for finding CO₂ 15- μ m band transmission in planetary atmospheres, *J. Geophys. Res.*, 91, 11,851–11,866, 1986.
- Edwards, J. M., and A. Slingo, Studies with a flexible new radiation code, I, Choosing a configuration for a large-scale model, *Q. J. R. Meteorol. Soc.*, 122, 689–719, 1996.
- Ellingson, R. G., and Y. Fouquart, The intercomparison of radiation codes in climate models: An overview, *J. Geophys. Res.*, 96, 8925–8927, 1991.
- Ellingson, R. G., and W. J. Wiscombe, The Spectral Radiance Experiment (SPECTRE): Project description and sample results, *Bull. Am. Meteorol. Soc.*, 77, 1967–1985, 1996.
- Ellingson, R. G., J. Ellis, and S. Fels, The intercomparison of radiation codes used in climate models: Long wave results, *J. Geophys. Res.*, 96, 8929–8933, 1991.
- Fu, Q., and K. N. Liou, On the correlated k -distribution method for radiative transfer in nonhomogeneous atmospheres, *J. Atmos. Sci.*, 49, 2139–2156, 1992.
- Gamache, R. R., R. L. Hawkins, and L. S. Rothman, Total internal partition sums in the temperature range 70–3000 K: Atmospheric linear molecules, *J. Mol. Spectrosc.*, 142, 205–219, 1990.
- Goody, R. M., A statistical model for water vapour absorption, *Q. J. R. Meteorol. Soc.*, 78, 165–169, 1952.
- Goody, R. M., R. West, L. Chen, and D. Crisp, The correlated k -distribution method for radiation calculation in nonhomogeneous atmospheres, *J. Quant. Spectrosc. Radiat. Transfer*, 42, 539–550, 1989.
- Kiehl, J. T., and V. Ramanathan, CO₂ radiative parameterization used in climate models: Comparison with narrowband models and with laboratory data, *J. Geophys. Res.*, 88, 5191–5202, 1983.
- Ko, M. K. W., H. R. Schneider, R.-L. Shia, D. K. Weisenstein, and N.-D. Sze, A two-dimensional model with coupled dynamics, radiation, and photochemistry, 1, Simulation of the middle atmosphere, *J. Geophys. Res.*, 98, 20,429–20,440, 1993.
- Kratz, D. P., B.-C. Gao, and J. T. Kiehl, A study of the radiative effects of the 9.4- and 10.4-micron bands of carbon dioxide, *J. Geophys. Res.*, 96, 9013–9020, 1991.
- Lacis, A. A., and J. E. Hansen, A parameterization for the absorption of solar radiation in the Earth's atmosphere, *J. Atmos. Sci.*, 31, 118–133, 1974.

- Lacis, A. A., and V. Oinas, A description of the correlated k -distribution method for modeling nongray gaseous absorption, thermal emission, and multiple scattering in vertically inhomogeneous atmospheres, *J. Geophys. Res.*, **96**, 9027–9074, 1991.
- Revercomb, H. E., F. A. Best, R. G. Dedecker, T. P. Dirks, R. A. Herbsleb, R. O. Knuteson, J. F. Short, and W. L. Smith, Atmospheric emitted radiance interferometer (AERI) for ARM, in *Fourth Symposium on Global Change Studies*, pp. 46–49, Am. Meteorol. Soc., Boston, Mass., 1993.
- Rothman, L. S., et al., HITRAN molecular database: Edition '92, *J. Quant. Spectrosc. Radiat. Transfer*, **48**, 469–507, 1992.
- Smith, W. L., H. E. Revercomb, H. B. Howell, and H. M. Woolf, HIS—A satellite instrument to observe temperature and humidity profiles with vertical resolution, paper presented at the Fifth Conference on Atmospheric Radiation, Am. Meteorol. Soc., Boston, Mass., 1983.
- Stokes, G. E., and S. E. Schwartz, The Atmospheric Radiation Measurement (ARM) Program: Programmatic background and design of the cloud and radiation test bed, *Bull. Am. Meteorol. Soc.*, **75**, 1201–1221, 1994.
- Toon, O. B., C. P. McKay, T. P. Ackerman, and K. Santhanam, Rapid calculation of radiative heating rates and photodissociation rates in inhomogeneous multiple scattering atmospheres, *J. Geophys. Res.*, **94**, 16,287–16,301, 1989.
- Wang, W. C., Y. L. Yung, A. A. Lacis, T. Mo, and J. E. Hansen, Greenhouse effects due to man-made perturbations of trace gases, *Science*, **194**, 685–690, 1976.
- West, R., D. Crisp, and L. Chen, Mapping transformations for broadband atmospheric radiation calculations, *J. Quant. Spectrosc. Radiat. Transfer*, **43**, 191–199, 1990.
- Wiscombe, W., and J. Evans, Exponential sum-fitting of radiative transmission functions, *J. Comput. Phys.*, **24**, 416–444, 1977.
- Zhu, X., On overlapping absorption of a gas mixture, *Theor. Appl. Climatol.*, **52**, 139–142, 1995.
- P. D. Brown, S. A. Clough, M. J. Iacono, and E. J. Mlawer, Atmospheric and Environmental Research, Inc., 840 Memorial Drive, Cambridge, MA 02139-3794.
- S. J. Taubman, Geophysical Fluid Dynamics Laboratory, Princeton, NJ 08540.

(Received August 12, 1996; revised December 30, 1996; accepted January 2, 1997.)